PLATE 3.3: Supply tank with oxygen meter in the foreground

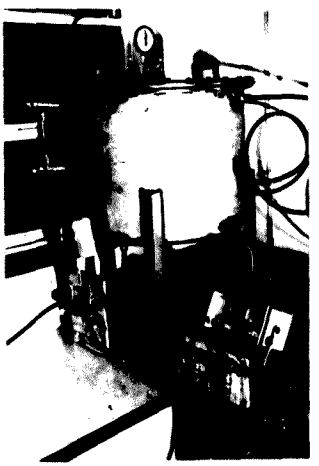

within the specification limits (O_2 < 100 ppb) for P.W.R. environments. The tank can then be pump mixed. A heater and heat exchanger are placed in line with the corrosion fatigue test cell to facilitate testing in hot aqueous solution.

The stainless steel tanks (450 ℓ and 200 ℓ) are manufactured from AISI 304L type stainless steel. Features in the design (Fig. 3.4) are:

1. A pressure gauge to measure the hydrogen over-pressure in the tanks.

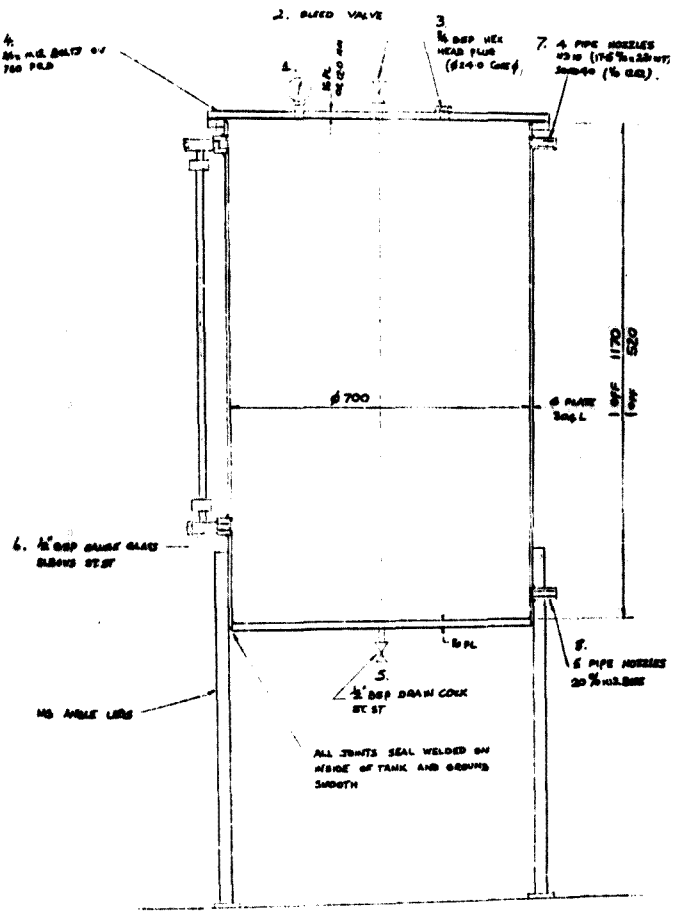

FIGURE 3.4: Stainless steel tanks

2. A relief valve which has a bursting pressure (variable setting) of 3 to 50 psi, through which H_2 is vented to atmosphere.

3. A hexagonal head plug which can be unscrewed for tank dosing.

4. Bolted lid which is seated on a soft neoprene rubber gasket. Neoprene provides a good seal and is one of the most resistant materials to oxygen through-diffusion.

5. Drain cock (ball valve) for emptying the tanks completely.

6. External glass level indicators with lower elbows containing ball valves to facilitate drainage of the glass tube.

7. All inlet and outlet parts consist of welded fittings attached to the tanks. Swagelok fittings are then screwed into these welded tubes. All weld beads are ground flush with the surface.

8. Entry port for hydrogen gas. The hydrogen passes into a H.D.P.E. (high density polyethylene) tube that consists of a coil full of tiny 'pin-prick' holes. This serves to distribute the hydrogen gas evenly and finely throughout the P.W.R. water. The lowering of the partial pressure of oxygen results in the lowering of oxygen contents in the water (Dalton's Law of partial gas pressures).

The content of the hydrogen cylinder has been analysed and found to be as follows.

oxygen	less than 3 vpm
moisture	less than 1 vpm
nitrogen	less than 2 vpm
carbon dioxide	less than 0.2 vpm
carbon monoxide	less than 0.2 vpm
hydrocarbons	less than 0.2 vpm
HYDROGEN	better than 99.9995%

9. The stainless steel tanks were chemically cleaned and pressure tested by the manufacturers. The maximum operating pressure is 16.9 bar (245 psig) for a maximum operating temperature of 66 °C (150 °F).

The 200 ℓ supply tank can be pump mixed using diaphragm pumps. This mini-recirculating loop has a sample point (simply a three-way valve system) so that samples can be taken to ensure thorough pump mixing. the design of all the return loops is such that the returning water 'cascades' through the hydrogen blanket thus facilitating dissolved oxygen removal.

The P.W.R. simulated water in the main supply loop is also pumped through a diaphragm pump. In fact, all the diaphragm pumps are driven by one motor (Plate 3.4). The pumping flowrates are variable and mixing can be carried out at flowrates for 0 to 626 ℓ/hr, this flowrate being produced by two pump heads. The first head can produce a maximum flowrate of 299 ℓ/hr and the second head a flowrate of 327 ℓ/hr. The corrosion fatigue test cell loop flowrates can be varied using the third pump head, giving a maximum flowrate of 144 ℓ/hr. All three pump heads have been tested to a pressure of 310.5 kPa. The P.W.R. water is in contact with polypropylene (diaphragm and pump body) with single nitrile rubber valve balls, glass plunger with single 'U' section nitrile rubber lipseal, i.e. all highly corrosion resisting materials.

The flowrate is controlled with a stroke length control setting. This is graduated to 100% of full stroke, which is the maximum flowrate and corresponds to a stroking distance of 7.5 mm for the diaphragm pumps. It should be noted that these pumps are actually metering pumps, but were found to be ideal for this type of service.

The main corrosion fatigue loop consists of another sampling point for chemical analysis checks and an in-line oxygen meter for batch analyses (Plate 3.5). A multiple valve assembly has been introduced near the test cell to facilitate sample changes and subsequent

PLATE 3.4: Diaphragm pumps:
- Single head for main loop recirculation
- Double head for tank mixing.

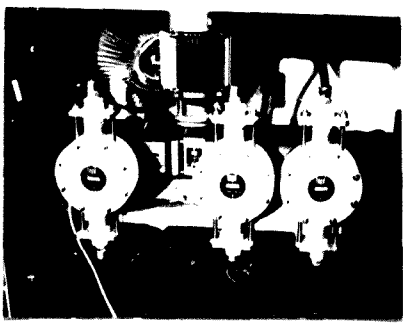

PLATE 3.5: Oxygen meter with sensor in the flow-through assembly

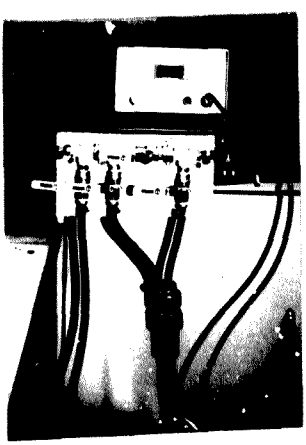

hydrogen purging without allowing the ingress of oxygen to the system.

Temperature variation tests, up to the boiling point of water, can be carried out using a heater and heat exchanger (Plate 3.6). The heater design consists of a tube (316 SS) ($^1/_2$ m long, O.D. = 168 mm, wall thickness = 7.1 mm) with flanges at either end (Fig. 3.5). Backing plates (10 mm thick) are bolted onto the flanges thus squeezing a nitrile rubber gasket to produce an air tight seal. The heating element, screwed into one of the blanking plates is a three-phase 6 kW heater, but only two phases will be used, thus making it a 4 kW heater. A simple energy balance assuming a typical flowrate of 25 ℓ/hr will show that water entering the heater at 25 °C will exit the heater at a temperature of approximately 163 °C ($Q = \dot{m}C\Delta T;C = 4.1796$ J/g °C). This calculation assumes that the heater will be on the whole time and that the water entering the heat exchanger will have a temperature of 25 °C. The entry temperature will be greater than 25 °C because of the use of a counter current heat exchanger, but more importantly the heater will be electrically controlled with a contactor.

PLATE 3.6: Cylindrical heater, plate heat exchanger and JENCO controller.

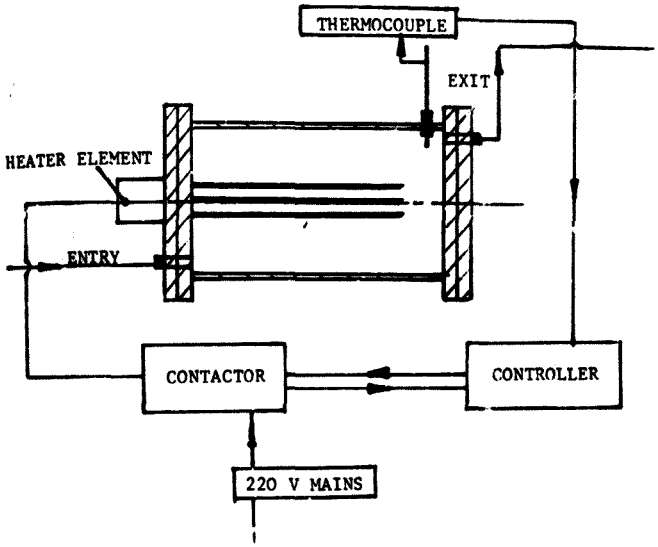

FIGURE 3.5: Heater assembly

A thermocouple fitting has been placed near the exit port of the heater (iron/constantan 371 JC type thermocouple). The thermocouple is then connected to a JIC JENCO 371 thermometer controller which will be set to the required temperature at the exit port of the heater (allowing for temperature losses before the water reaches the cell). The temperature in the test cell is also monitored by a thermocouple/L.E.D. display unit and therefore an easy calibration can be done in order to set the controller temperature to the required value.

The controller is in turn linked to a 4A/40A contacter which is connected to the heating element. Thus if the temperature is too

low (as registered by the thermocouple) the controller activates the contacter which results in the contacting of the heater to the mains power. Once the temperature is correct, the heater is deactivated. A 4 A/40 A contacter is required to convert the controller signal 4 A into a signal 'acceptable' to the heater (220 V; 4 kW . $P = VI$ therefore $I = 18.2$ A required). Clearly such a system must be overdesigned!

The heated water passes into the test cell and returns to the storage tank via a 0.2 μm filter and a heat exchanger. The heat exchanger is a plate heat exchanger which has been designed on the following criteria:

For a water flowrate of 0.01 kg/s

Temperature programme: Inlet water of 20 °C will be heated to 90 °C before entry into the cell. The water exiting the cell and entering the counter flow heat exchanger having a temperature of 95 °C (after heater) will be cooled to 25 °C before re-entry to the tank.

The main requirement of the heat exchanger is for the return water to be cooled to below 40 °C, which is the maximum (temperature of water) that can flow through the water treatment plant (should the water purification unit be placed in-line). This would only need to be used if the water needs to be reconditioned.

Figures 3.6, 3.7 and 3.8 show the heat exchanger design and water flow directions. The heat exchanger plates are corrugated for two reasons:

- To promote turbulance in the fluid flowing between them, and
- To support the plates against different pressures.

The plate material is 0.6 mm A.I.S.I. type 316 austenitic stainless steel and the gasket material is resin-cured butyl rubber which has an extremely low O_2 diffusion rate. The combination of high heat

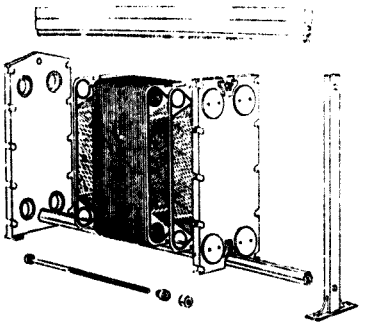

FIGURE 3.6: Plate heat exchanger

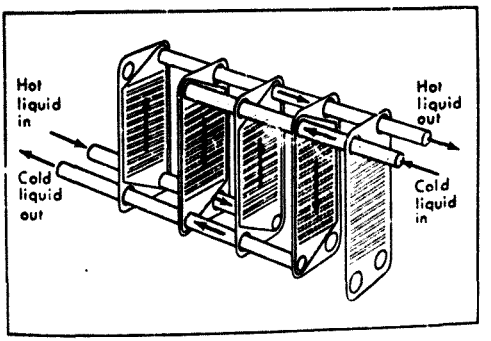

FIGURE 3.7: Plate heat exchanger includes corrugated plates, gaskets, frame, and corner portals to achieve desired flow.

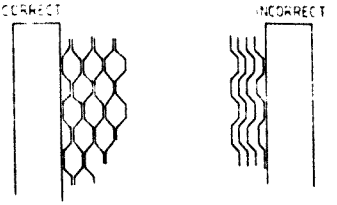

NOTE CORRECT METHOD SHOWING HONEYCOMB EFFECT ON THE LEFT THIS MAKES FOR COMPLETE GASKET SEALING AND CORRECT PLATE PACK ASSEMBLY

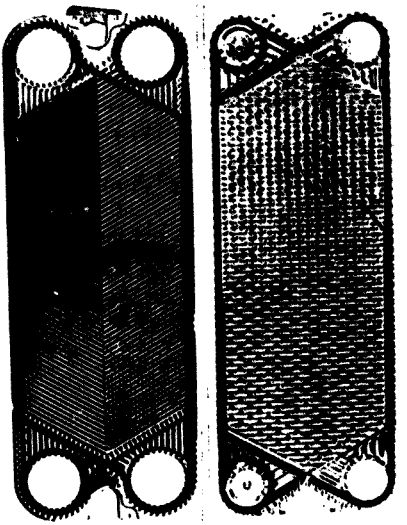

FIGURE 3.8: Corrugated metal sheets are clamped together in plate heat exchangers to provide flow channels.

transfer coefficient, advantageous flow ratio characteristics and full countercurrent flow makes it possible to achieve very close approach temperatures and high degrees of temperature cross-over. Over 90% heat recovery is possible when using a single plate heat exchanger. The maximum operation temperature is 130 °C (for the rubber gaskets).

All piping consists of L.D.P.E. (low density polyethylene) which has a permeability (to O_2) of only 60 x 10^{-10} cc.mm/sec.cm^2.cmHg. Assuming a tube to have a length of 50 m with an O.D. of $^1/_2$", I.D. of $^3/_8$", a simple calculation will show that in six months the O_2 leaking into 160 ℓ of P.W.R. water will be 0.1 ppb which, can be regarded as negligible in a specification of up to 100 ppb dissolved oxygen.

3.2.1 Corrosion Fatigue Test Cell

Corrosion fatigue testing is carried out in a Perspex cell. The cell was designed to incorporate the maximum amount of flexibility [49] to the testing programme as well as remaining chemically inert in the 'low' temperature P.W.R. water environment. The cell facilitated optical crack length measurement as well as potential drop (P.D.) crack length measurement (discussed later). The cell design drawing is shown in Fig. 3.9.

The 12 mm thick Perspex cell provides a good barrier against the ingress of oxygen tc the test environment. Rubber O-ring seals (on all parts) prevent the leakage of P.W.R. type water and also prevent the ingress of oxygen to the water.

The cell includes ports for P.D. crack length measurement leads, water inlet and outlet, thermocouple insertion and clevis (loading rod) positioning. Side plates can he unbolted so that specimens can be changed with the minimum disruption to the cell set-up procedure. Plates 3.7 and 3.8 show a photograph of he test cell arrangement. The P.W.R. water enters the bottom of the cell and exits at the top where the water is returned to the storage tank.

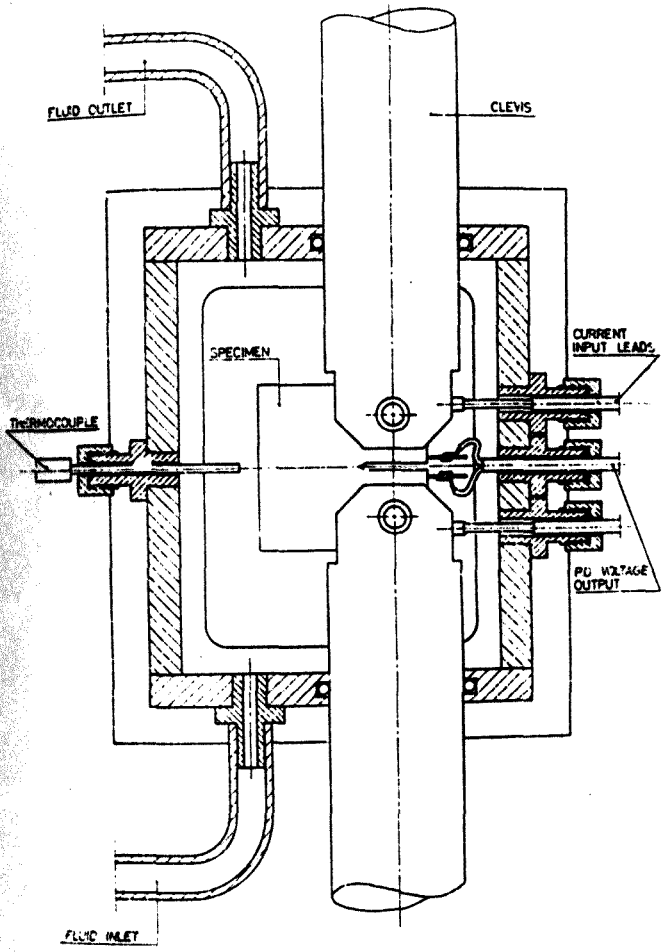

FIGURE 3.9: Corrosion fatigue test cell

PLATE 3.7: Test cell for corrosion fatigue testing in P.W.R. environments.

PLATE 3.8: Test cell with optical crack length measuring device, Luggin probe with Calomel Electrode insert.

3.2.2 Mechanical Testing Apparatus and Control

Fatigue testing is carried out on a 50 kN capacity E.S.H. servo-hydraulic testing machine (Plate 3.9). The closed loop servo system for the servo-controlled electro-hydraulic testing machine is shown in Fig. 3.10.

The desired signal is transmitted to the servo-controller which activates the loading cylinder. Such a system has the advantage that a large variety of signals can be passed through the servo-system. This produces considerable flexibility, enabling it to accommodate many specimen configurations. A waveform generator is employed to create both sine waves and positive sawtooth waveforms at high frequencies.

A Commodore Pet microcomputer is used to control the fatigue testing. The computer stores crack growth rate data on disk so that test data can be analysed at a later stage. The computer control proved necessary because some of the tests lasted for up to one week. Clearly manual operation would be most arduous.

The computer is also used to generate waveforms when low frequency testing was undertaken. For such testing the waveform generator is not required. The output signal is relayed from the computer to the E.S.H testing machine via an interface unit. This is carried out while the computer monitors the E.S.H. output signal, returned back to the computer via the interface unit. The computer monitored: the number of cycles, the voltage from the crack length measurement unit (and subsequently the computed crack length). When the computer generates the waveforms (low frequencies), related to an interfacing constraint, crack length measurement is undertaken at discrete intervals. During these intervals fatiguing is stopped momentarily and the loads are reduced to the mean level.

3.2.2.1 Crack length measurement

The D.C. potential drop technique for crack length measurement has proved to be a flexible, cheap and an easily automated means of

PLATE 3.9: 50 kN E.S.H. testing machine and controls

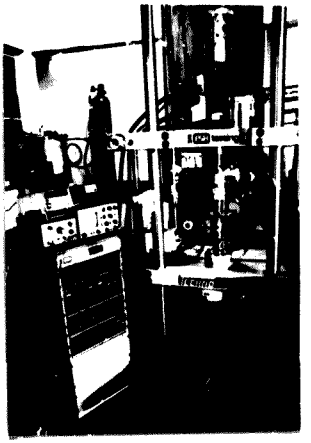

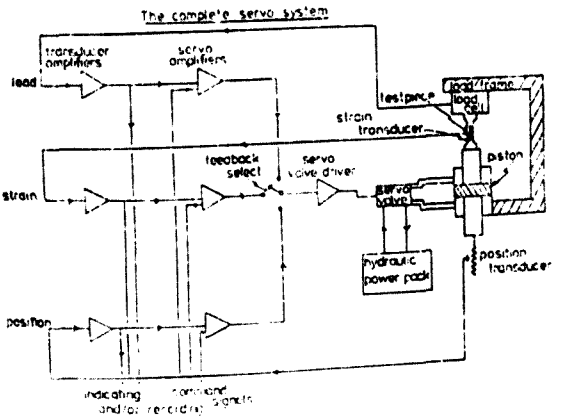

FIGURE 3.10: Closed-loop servo system

crack length monitoring. The method relies on an increase in specimen resistance across the remaining ligament in a cracking specimen. By applying a constant current through the specimen, the potential difference between probes attached across the crack will increase as the cross-sectional area decreases with crack extension. By monitoring the potential difference between two points either side of the crack (Fig. 3.11) and comparing it with that at the start of the test as well as visual crack length determination, the crack length may be accurately determined during the fatigue test.

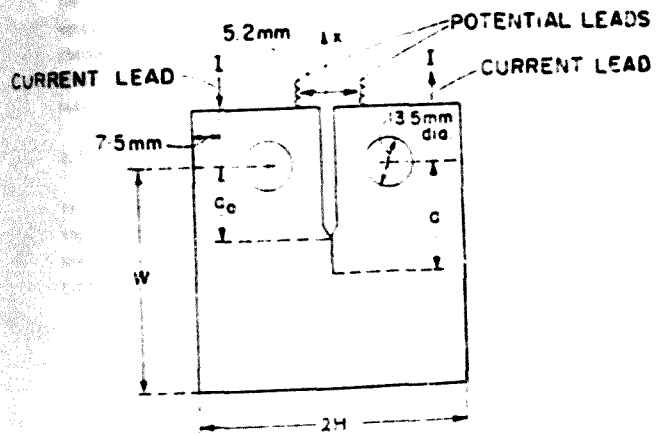

FIGURE 3.11: C.T. specimen showing the location of current input and potential measurement leads.

A Farnell constant current supply unit was used to provide a highly stabilized current. The current carrying leads were attached to the specimen with aluminium screwed connections which provide a

good conductivity input to the sample. The choice of current (20 A) was found to give good voltage output and minimal thermo-electric heating.

Probe wires for measurement of potential drop, typically about 0.2 mm diameter were attached to wire-wrapping pins inserted in the specimens. These pins were inserted by drilling 0.8 mm diameter holes 2 mm either side of the notch centre. While crack length was monitored using the P.D. method, surface crack length measurements were also taken for calibration purposes (x10 magnification travelling microscopes).

The Fluke 8860A digital multimeter was used for potential measurement. The meter offers high resolution in order to detect small changes in crack length, especially for small cracks i.e. the start of crack growth. The Fluke also interfaces well with the micro computer so that remote control and data logging can be carried out.

3.3 ANALYTICAL EQUIPMENT

In order to check the water chemistry characteristics of the testing 'P.W.R.' type water, it was necessary to purchase or gain the use of some sophisticated analytical equipment. The recent round robin test specification set up by the I.C.C.G.R. was as follows:

Water Chemistry	P.W.R. Tests
Conductivity	<20 μmho/cm
pH (room temperature)	6.5 ± C.2
Dissolved O_2	<5 ppb
Boron	1000 ppm
H_2	15-50 std.cc/kg H_2O
Chloride	<0.1 ppm
Fluoride	<0.1 ppm

Clearly, for such low concentrations, accurate analytical techniques are required. In addition, it is now a requirement that sulphate levels be accurately measured.

3.3.1 Conductivity (Orion model 101 Conductivity Meter)

The Orion model 101 conductivity meter is a research quality meter which can be used to measure electrical conductance in a wide range of conditions (Plate 3.10). Measurement of conductance can be made from 0.001 µmho to 1 mho using a variety of cells with an accuracy better than 1% of full scale.

PLATE 3.10: Orion conductivity meter and electrode

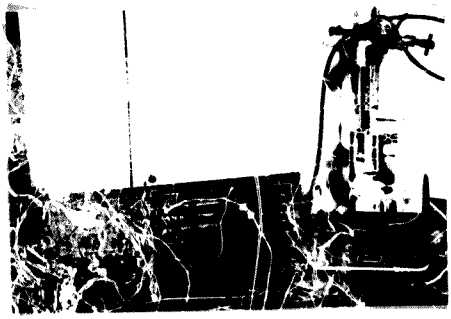

The conductance, being the ability of a solution to conduct a current, is expressed in reciprocal ohms or mhos. The term conductance is preferred and is reported in micro-mhos per centimeter (µmhos/cm). In the international system of units (S.I.) the reciprocal of the ohm is the siemen (S).

The Orion 101, when used with the appropriate %T coefficient and the sample temperature controls, can display the conductance automatically converted to 25 °C. The conductance can be continuously observed by means of a recorder through the recorder output, or by digital linking to micro-processors and computers.

The Orion model 101 allows selection of three A.C. frequencies (3 kHz, 1 kHz, 80 Hz) permitting a choice of cell types. It consists of an oscillator, amplifier and synchronous detector. The D.C. output is proportional to cell conductance, with minimum interference from capacitance because of the synchronous detector. The electronic design permits the use of any electrically conducting material for electrode construction, the only limitations being corrosion by the solution to be measured.

Before making measurements, it is important to select the appropriate working frequency. Cells with platinized electrodes are calibrated at 1 kHz; therefore the most accurate conductance measurements will be made at the same frequency. The 3 kHz frequency should be used when working with special cells with steel electrodes. The 80 Hz frequency is recommended for conductance measurements at very low levels (on the order of μmhos). When operating at low levels, it is necessary to use cells with very small cell constants (0.1), which consequently have large capacitive effects.

Temperature compensation is achieved by using the %T coefficient per °C control. The Orion 101 solves the following equation:

$$K_{25\,^\circ C} = \frac{K_t}{1 + \alpha (t - 25)}$$

$K_{25\,^\circ C}$ = specific conductance at 25 °C
K_t = specific conductance at sample temperature
α = temperature coefficient
t = temperature of sample.

Conductance at infinite dilution increases with increasing temperatures according to the equation above. For salts the α value, converted to a percent value, varies between 1.9% and [illegible], so that the conductance varies approximately 2% per °C. Acids and bases have a lower temperature coefficient (1.6% for acids, ± 1.8% for bases). In general, the greater the ion's mobility the less its temperature coefficient. Mobility differences between different ions decreases when temperature increases.

Table 3.1 shows examples of some conductivity measurements. Included are recommended cell constants and measuring frequencies.

Table 3.2 shows a cell and frequency selection chart for the 101 model conductivity meter.

TABLE 3.2: Cell and Frequency Selection Chart

Range	Frequency (1)			Cell Constant		
	80 Hz	1 kHz	3 kHz	0.1	1.0	10
1 mho		x	x		x	x
100 mmho		x	x		x	x
10 mmho		x	x		x	x
1 mmho	x	x	x		x	
100 µmho	x	x	x	x	x	
10 µmho	x	display	display	x	x	
1 µmho	x	blanks	blanks	x	x	

NOTE: 3 kHz should be used with steel cells only.

Over-range is indicated by blinking of the display. When ranges 1 µmho and 10 µmho are selected only the frequency 80 Hz can operate. When 3 kHz or 1 kHz is selected there is no display.

TABLE 3.1

Resistivity	100,000,000	10,000,000	1,000,000	100,000	10,000	1,000	100	10	1	Ohm.cm
Conductivity	0,01	0,1	1	10	100	1,000	10,000	100,000	1,000,000	$\mu S\ cm^{-1}$
Example	Ultre pure water		Good distilled water		Good drinking water	0,01% HCl			30% H_2SO_4	
Cell constant	0,01	0,1	1		10					
Measuring frequency	Low frequency				High frequency				4-electrode measurement	

3.3.2 High Sensitivity Dissolved Oxygen Detector (Plate 3.5)

The sensor of the Orbisphere Model 2713 oxygen detector is of the membrane enclosed polargraphic type. It senses the presence of oxygen in a medium contacting the membrane, and passes a current to the measuring instrument, which is precisely proportional to the concentration of this oxygen throughout the range from 1 µg/ℓ (1 ppb) to 20 µg/ℓ (20 ppm).

The instrument possesses four measurement scales; 0 - 20, 0 - 2, 0 - 0.2 and 0 - 0.02 µg/ℓ, for the accurate display of any concentration in this range. Range selection is made automatically by an internal autoranging circuit. Calibration is easily performed by exposing the sensor to water saturated air and adjusting the meter indication, with the gain control to a value available from tables shown overleaf (Table 3.3).

The instrument measures temperature by means of a thermister located within the sensor. The temperature signal may be displayed by selecting the °C position of the function switch and in addition is continuously available, together with the oxygen signal, at a recorder output connection. It is valid within the range 0 - 45 °C and has an accuracy of ±0.2 °C. A flow chamber enables the sensor to be mounted in an airtight flow circuit, for the continuous monitoring of oxygen levels in a pumped sample stream. Sample flowrates should be within the range of 50 cm^3/min to 250 cm^3/min and sample temperatures may be anywhere within the range 0 - 45 °C, though a sample temperature of 20 °C to 25 °C will result in optimum performance. Sample pressure should be less than 20 bar. Figure 3.12 shows a view of the oxygen sensor and Fig. 3.13 is a schematic diagram showing the oxygen sensor and the flow chamber (all dimensions in mm).

TABLE 3.3: Oxygen solubility in air saturated fresh water (mg/L)

Temp (C)	Pressure (Torr)										
	600	605	610	615	620	625	630	635	640	645
0	11.48	11.58	11.67	11.77	11.87	11.96	12.06	12.16	12.25	12.35
1	11.17	11.26	11.36	11.45	11.54	11.64	11.73	11.82	11.92	12.01
2	10.87	10.96	11.05	11.14	11.23	11.32	11.42	11.51	11.60	11.69
3	10.58	10.67	10.76	10.85	10.94	11.03	11.11	11.20	11.29	11.38
4	10.30	10.39	10.48	10.56	10.65	10.74	10.82	10.91	11.00	11.08
5	10.04	10.12	10.21	10.29	10.37	10.46	10.54	10.63	10.71	10.80
6	9.78	9.86	9.95	10.03	10.11	10.19	10.28	10.36	10.44	10.52
7	9.54	9.62	9.70	9.78	9.86	9.94	10.02	10.10	10.18	10.26
8	9.30	9.38	9.46	9.54	9.61	9.69	9.77	9.85	9.93	10.01
9	9.07	9.15	9.23	9.30	9.38	9.46	9.53	9.61	9.69	9.76
10	8.86	8.93	9.01	9.09	9.16	9.23	9.31	9.39	9.46	9.53
11	8.66	8.72	8.80	8.87	8.94	9.02	9.09	9.16	9.24	9.31
12	8.45	8.52	8.59	8.66	8.74	8.81	8.88	8.95	9.02	9.09
13	8.26	8.33	8.40	8.47	8.54	8.61	8.68	8.75	8.82	8.89
14	8.07	8.14	8.21	8.28	8.35	8.42	8.49	8.55	8.62	8.69
15	7.90	7.96	8.03	8.10	8.16	8.23	8.30	8.37	8.43	8.50
16	7.72	7.78	7.86	7.92	7.99	8.05	8.12	8.19	8.25	8.32
17	7.56	7.63	7.69	7.75	7.82	7.88	7.95	8.01	8.08	8.14
18	7.40	7.47	7.53	7.59	7.66	7.72	7.78	7.85	7.91	7.97
19	7.25	7.31	7.38	7.44	7.50	7.56	7.62	7.69	7.75	7.81
20	7.11	7.17	7.23	7.29	7.35	7.41	7.47	7.53	7.59	7.65
21	6.96	7.02	7.08	7.14	7.20	7.26	7.32	7.38	7.44	7.50
22	6.83	6.89	6.95	7.00	7.06	7.12	7.18	7.24	7.30	7.36
23	6.70	6.75	6.81	6.87	6.93	6.99	7.04	7.10	7.16	7.22
24	6.5	6.63	6.69	6.74	6.80	6.85	6.91	6.97	7.03	7.08
25	6.46	6.50	6.56	6.62	6.67	6.73	6.78	6.84	6.90	6.95
26	6.33	6.38	6.44	6.49	6.55	6.60	6.66	6.71	6.77	6.82
27	6.21	6.27	6.32	6.38	6.43	6.49	6.54	6.60	6.65	6.70
28	6.10	6.16	6.21	6.26	6.32	6.37	6.43	6.48	6.53	6.58
29	5.99	6.05	6.13	6.15	6.21	6.25	6.31	6.36	6.42	6.47
30	5.89	5.94	5.99	6.05	6.10	6.15	6.20	6.25	6.30	6.36
31	5.79	5.84	5.89	5.94	5.99	6.04	6.09	6.15	6.20	6.25
32	5.69	5.74	5.79	5.84	5.89	5.94	5.99	6.05	6.09	6.15
33	5.59	5.65	5.69	5.75	5.79	5.84	5.89	5.94	5.99	6.04
34	5.50	5.54	5.59	5.64	5.69	5.74	5.79	5.84	5.89	5.94
35	5.40	5.45	5.50	5.55	5.59	5.64	5.69	5.74	5.79	5.84
36	5.31	5.36	5.41	5.45	5.50	5.55	5.59	5.65	5.69	5.74
37	5.22	5.27	5.32	5.36	5.41	5.46	5.51	5.55	5.60	5.65
38	5.13	5.18	5.23	5.27	5.32	5.37	5.41	5.46	5.51	5.55
39	5.05	5.09	5.14	5.19	5.23	5.28	5.32	5.37	5.42	5.46
40	4.96	5.01	5.06	5.10	5.15	5.19	5.24	5.29	5.33	5.37

Temp (C)	Pressure (Torr)									
	600	605	610	615	620	625	630	635	640	645
41	4.88	4.92	4.97	5.01	5.06	5.11	5.15	5.20	5.24	5.29
42	4.80	4.84	4.89	4.93	4.98	5.02	5.06	5.11	5.15	5.20
43	4.72	4.76	4.80	4.85	4.89	4.94	4.98	5.02	5.07	5.11
44	4.64	4.68	4.72	4.77	4.81	4.85	4.90	4.94	4.98	5.03
45	4.56	4.60	4.64	4.68	4.73	4.77	4.81	4.86	4.90	4.94
46	4.48	4.52	4.56	4.60	4.65	4.69	4.73	4.77	4.82	4.86
47	4.40	4.44	4.49	4.52	4.57	4.61	4.65	4.69	4.74	4.78
48	4.32	4.36	4.40	4.45	4.49	4.53	4.57	4.61	4.66	4.70
49	4.24	4.28	4.33	4.37	4.41	4.45	4.49	4.53	4.57	4.62
50	4.17	4.21	4.25	4.29	4.33	4.37	4.41	4.45	4.49	4.53
	650	655	660	665	670	675	680	685	690	695
0	12.44	12.54	12.64	12.73	12.83	12.93	13.02	13.12	13.22	13.31
1	12.11	12.20	12.29	12.39	12.48	12.58	12.67	12.76	12.86	12.95
2	11.78	11.87	11.96	12.06	12.15	12.24	12.33	12.43	12.52	12.61
3	11.47	11.56	11.65	11.74	11.83	11.91	12.00	12.09	12.18	12.27
4	11.17	11.26	11.34	11.43	11.52	11.60	11.69	11.78	11.86	11.95
5	10.88	10.97	11.06	11.14	11.23	11.31	11.40	11.47	11.56	11.64
6	10.61	10.69	10.77	10.85	10.94	11.02	11.10	11.19	11.27	11.35
7	10.34	10.42	10.50	10.58	10.66	10.74	10.82	10.90	10.98	11.06
8	10.09	10.16	10.24	10.32	10.40	10.48	10.56	10.64	10.71	10.79
9	9.84	9.92	9.99	10.07	10.15	10.22	10.30	10.38	10.46	10.53
10	9.61	9.68	9.76	9.83	9.91	9.98	10.06	10.13	10.21	10.29
11	9.39	9.46	9.53	9.61	9.68	9.75	9.83	9.90	9.97	10.04
12	9.17	9.24	9.31	9.38	9.45	9.53	9.60	9.67	9.74	9.81
13	8.96	9.03	9.10	9.17	9.24	9.31	9.38	9.45	9.52	9.59
14	8.76	8.83	8.90	8.97	9.03	9.10	9.17	9.24	9.31	9.38
15	8.57	8.63	8.70	8.77	8.83	8.90	8.97	9.04	9.11	9.17
16	8.38	8.44	8.51	8.57	8.64	8.71	8.77	8.84	8.91	8.97
17	8.21	8.27	8.33	8.40	8.46	8.53	8.59	8.66	8.72	8.78
18	8.04	8.10	8.16	8.23	8.29	8.35	8.42	8.48	8.54	8.61
19	7.87	7.93	7.99	8.06	8.12	8.18	8.24	8.30	8.36	8.43
20	7.72	7.78	7.84	7.90	7.96	8.02	8.08	8.14	8.20	8.26
21	7.56	7.62	7.68	7.74	7.80	7.86	7.92	7.98	8.04	8.10
22	7.41	7.47	7.53	7.59	7.65	7.71	7.77	7.83	7.89	7.95
23	7.26	7.32	7.38	7.44	7.50	7.56	7.62	7.68	7.74	7.80
24	7.14	7.20	7.26	7.31	7.37	7.43	7.49	7.55	7.61	7.67
25	7.01	7.06	7.12	7.18	7.24	7.30	7.36	7.42	7.48	7.54
26	6.88	6.94	7.00	7.06	7.12	7.18	7.24	7.30	7.36	7.42
27	6.76	6.82	6.88	6.94	7.00	7.06	7.12	7.18	7.24	7.30
28	6.64	6.70	6.76	6.82	6.88	6.94	7.00	7.06	7.12	7.18
29	6.53	6.59	6.65	6.71	6.77	6.83	6.89	6.95	7.01	7.07
30	6.42	6.48	6.54	6.60	6.66	6.72	6.78	6.84	6.90	6.96
31	6.32	6.38	6.44	6.50	6.56	6.62	6.68	6.74	6.80	6.86
32	6.22	6.28	6.34	6.40	6.46	6.52	6.58	6.64	6.70	6.76
33	6.12	6.18	6.24	6.30	6.36	6.42	6.48	6.54	6.60	6.66
34	6.03	6.09	6.15	6.21	6.27	6.33	6.39	6.45	6.51	6.57
35	5.94	6.00	6.06	6.12	6.18	6.24	6.30	6.36	6.42	6.48
36	5.85	5.91	5.97	6.03	6.09	6.15	6.21	6.27	6.33	6.39
37	5.76	5.82	5.88	5.94	6.00	6.06	6.12	6.18	6.24	6.30
38	5.68	5.74	5.80	5.86	5.92	5.98	6.04	6.10	6.16	6.22
39	5.60	5.66	5.72	5.78	5.84	5.90	5.96	6.02	6.08	6.14
40	5.52	5.58	5.64	5.70	5.76	5.82	5.88	5.94	6.00	6.06
41	5.44	5.50	5.56	5.62	5.68	5.74	5.80	5.86	5.92	5.98
42	5.36	5.42	5.48	5.54	5.60	5.66	5.72	5.78	5.84	5.90
43	5.29	5.35	5.41	5.47	5.53	5.59	5.65	5.71	5.77	5.83
44	5.22	5.28	5.34	5.40	5.46	5.52	5.58	5.64	5.70	5.76
45	5.15	5.21	5.27	5.33	5.39	5.45	5.51	5.57	5.63	5.69
46	5.08	5.14	5.20	5.26	5.32	5.38	5.44	5.50	5.56	5.62
47	5.01	5.07	5.13	5.19	5.25	5.31	5.37	5.43	5.49	5.55
48	4.94	5.00	5.06	5.12	5.18	5.24	5.30	5.36	5.42	5.48
49	4.87	4.93	4.99	5.05	5.11	5.17	5.23	5.29	5.35	5.41
50	4.81	4.87	4.93	4.99	5.05	5.11	5.17	5.23	5.29	5.35

Temp (C)	Pressure (Torr)									
	650	655	660	665	670	675	680	685	690	695
31	6.30	6.35	6.40	6.45	6.50	6.55	6.61	6.36	6.71	6.76
32	6.16	6.24	6.29	6.34	6.39	6.44	6.49	6.54	6.59	6.65
33	6.09	6.14	6.19	6.24	6.29	6.34	6.39	6.44	6.49	6.54
34	5.7	6.04	6.08	6.13	6.18	6.23	6.28	6.33	6.38	6.43
35	5.89	5.94	5.98	6.03	6.08	6.13	6.18	6.23	6.27	6.32
36	5.79	5.84	5.89	5.93	5.98	6.03	6.08	6.12	6.17	6.22
37	5.69	5.74	5.79	5.84	5.88	5.93	5.98	6.03	6.07	6.12
38	5.60	5.65	5.69	5.74	5.79	5.83	5.88	5.93	5.97	6.02
39	5.51	5.56	5.60	5.65	5.69	5.74	5.79	5.83	5.88	5.92
40	5.42	5.47	5.51	5.56	5.60	5.65	5.69	5.74	5.78	5.83
41	5.3x	5.38	5.42	5.47	5.51	5.56	5.60	5.65	5.69	5.74
42	5.24	5.29	5.33	5.38	5.42	5.47	5.51	5.55	5.60	5.64
43	5.16	5.20	5.24	5.29	5.33	5.38	5.42	5.46	5.51	5.55
44	5.07	5.11	5.1	[illegible]	5.25	5.29	5.33	5.38	5.42	5.46
45	4.99	5.03	[illegible]	[illegible]	[illegible]6	5.20	5.25	5.29	5.33	5.37
46	4.90	4	[illegible]	[illegible]	[illegible]	5.12	5.16	5.20	5.24	5.29
47	4.82	4.8	[illegible]	[illegible]	[illegible]	5.03	5.07	5.12	5.16	5.20
48	4.74	4	[illegible]	[illegible]	91	4.95	4.99	5.03	5.07	5.11
49	4.66	4.7	[illegible]	[illegible]	82	4.86	4.91	4.95	4.99	5.03
50	4.58	4.62	4.6	[illegible]	74	4.78	4.82	4.86	4.90	4.95
	700	705	710	715	720	725	730	735	740	745
0	13.41	13.51	13.60	13.70	13.80	13.89	13.99	14.08	14.18	14.28
1	13.05	13.14	13.23	13.33	13.42	13.51	13.61	13.70	13.80	13.89
2	12.70	12.79	12.88	12.97	13.06	13.15	13.24	13.34	13.43	13.52
3	12.36	12.45	12.54	12.63	12.72	12.80	12.89	12.98	13.07	13.16
4	12.04	12.12	12.21	12.30	12.38	12.47	12.56	12.64	12.73	12.82
5	11.73	11.81	11.90	11.98	12.07	12.16	12.23	12.32	12.40	12.49
6	11.48	11.91	11.80	11.68	11.86	11.94	11.93	12.01	12.09	12.17
7	11.15	11.23	11.31	11.39	11.47	11.55	11.63	11.71	11.79	11.87
8	10.87	10.95	11.03	11.11	11.19	11.26	11.34	11.42	11.50	11.58
9	10.61	10.69	10.76	10.84	10.92	10.99	11.07	11.15	11.22	11.30
10	10.36	10.43	10.91	10.58	10.66	10.73	10.81	10.88	10.96	11.03
11	10.11	10.19	10.26	10.33	10.41	10.48	10 55	10.63	10.70	10.77
12	9.88	9.95	10.03	10.10	10.17	10 24	10.31	10.38	10.46	10.53
13	9.66	9.73	9.80	9.87	9.94	10.01	10.08	10.15	10.22	10.29
14	9.45	9.51	9.58	9.65	9.72	9.79	9.86	9.93	9.99	10.06
15	9.24	9.31	9.37	9.44	9.51	9 58	9.64	9.71	9.78	9.84
16	9.04	9.11	9.17	9.24	9.31	9.37	9.44	9.50	9.57	9.64
17	8.85	8.92	8.98	9.05	9.11	9.18	9.24	9.30	9.37	9.43
18	8.67	8.73	8.80	8.86	8.92	8.98	9.05	9.11	9.18	9.24
19	8.49	8.56	8.62	8.68	8.74	8.80	8.87	8.93	8.99	9.05
20	8.33	8.39	8.45	8.51	8.57	8.63	8.69	8 75	8.81	8.87

Temp (C)	Pressure (Torr)									
	700	705	710	715	720	725	730	735	740	745
21	8.16	8.22	8.28	8.34	8.40	8.46	8.52	8.58	8.64	8.70
22	8.01	8.08	8.12	8.18	8.24	8.30	8.36	8.42	8.48	8.54
23	7.85	7.91	7.97	8.03	8.09	8.16	8.20	8.26	8.32	8.37
24	7.71	7.76	7.82	7.88	7.94	7.99	8.05	8.11	8.16	8.22
25	7.57	7.62	7.68	7.73	7.79	7.85	7.90	7.96	8.01	8.07
26	7.43	7.49	7.54	7.60	7.65	7.71	7.76	7.82	7.87	7.93
27	7.30	7.35	7.41	7.46	7.52	7.57	7.62	7.68	7.73	7.78
28	7.17	7.22	7.28	7.33	7.38	7.44	7.49	7.54	7.60	7.65
29	7.05	7.10	7.15	7.20	7.25	7.3	7.36	7.41	7.47	7.52
30	6.93	6.98	7.03	7.08	7.13	7.19	7.24	7.29	7.34	7.39
31	6.81	6.86	6.91	6.96	7.01	7.06	7.12	7.17	7.22	7.27
32	6.70	6.75	6.80	6.84	6.90	6.95	7.00	7.05	7.10	7.16
33	6.58	6.63	6.68	6.73	6.78	6.83	6.88	6.93	6.99	7.03
34	6.48	6.53	6.57	6.62	6.67	6.72	6.77	6.82	6.87	6.92
35	6.37	6.42	6.47	6.52	6.56	6.61	6.66	6.71	6.76	6.81
36	6.27	6.32	6.36	6.41	6.46	6.51	6.56	6.60	6.65	6.70
37	6.17	6.21	6.26	6.31	6.36	6.40	6.45	6.50	6.54	6.59
38	6.07	6.11	6.16	6.21	6.25	6.30	6.35	6.39	6.44	6.49
39	5.97	6.02	6.06	6.11	6.15	6.20	6.24	6.29	6.34	6.39
40	5.88	5.92	5.97	6.01	6.06	6.10	6.15	6.19	6.24	6.29
41	5.78	5.83	5.87	5.92	5.96	6.01	6.05	6.10	6.14	6.19
42	5.69	5.73	5.78	5.82	5.87	5.91	5.96	6.00	6.04	6.09
43	5.60	5.64	5.69	5.73	5.77	5.82	5.86	5.91	5.95	5.99
44	5.51	5.55	5.59	5.64	5.68	5.73	5.77	5.81	5.86	5.90
45	5.42	5.46	5.50	5.55	5.59	5.63	5.68	5.72	5.76	5.81
46	5.33	5.37	5.42	5.46	5.50	5.54	5.59	5.63	5.67	5.71
47	5.24	5.28	5.33	5.37	5.41	5.45	5.50	5.54	5.58	5.62
48	5.16	5.20	5.24	5.28	5.32	5.37	5.41	5.45	5.50	5.54
49	5.07	5.11	5.15	5.20	5.24	5.28	5.32	5.37	5.41	5.45
50	4.99	5.03	5.07	5.11	5.15	5.19	5.23	5.27	5.31	5.36
	750	755	760	765	770	775	780	785	790	795
0	10.37	10.43	10.37	10.06	11.74	11.46	11.95	12.05	11.18	11.24
1	11.00	11.06	11.17	11.17	11.36	11.41	11.55	11.64	11.73	11.83
2	11.61	11.70	11.79	11.888	11.97	11.47	12.10	12.25	12.36	12.43
3	12.25	12.36	12.45	12.57	12.67	12.66	12.78	12.87	12.98	13.05
4	12.90	13.00	13.09	13.16	13.25	13.36	13.47	13.51	13.60	13.68
5	13.47	13.48	13.78	13.83	13.91	13.99	14.08	14.18	14.29	14.33
6	13.76	13.81	13.87	13.90	13.98	14.07	14.16	14.23	14.31	14.39
7	14.04	14.11	14.17	14.23	14.31	14.39	14.47	14.55	14.63	14.71
8	14.32	14.39	14.45	14.51	14.59	14.67	14.75	14.83	14.91	14.99
9	14.59	14.66	14.72	14.78	14.86	14.94	15.02	15.10	15.18	15.26
10	14.86	14.93	14.99	15.05	15.13	15.21	15.29	15.37	15.45	15.53
11	10.98	10.99	10.99	11.07	11.14	11.21	11.29	11.36	11.43	11.51
12	10.60	10.67	10.74	10.81	10.88	10.96	11.03	11.10	11.17	11.25
13	10.36	10.43	10.50	10.57	10.64	10.71	10.78	10.85	10.92	10.99
14	10.13	10.20	10.27	10.34	10.41	10.48	10.55	10.61	10.68	10.75
15	9.91	9.98	10.05	10.11	10.18	10.25	10.32	10.38	10.45	10.52
16	9.70	9.77	9.83	9.90	9.96	10.03	10.10	10.16	10.23	10.30
17	9.50	9.56	9.63	9.69	9.76	9.82	9.89	9.95	10.01	10.08
18	9.30	9.37	9.43	9.49	9.56	9.62	9.68	9.75	9.81	9.87
19	9.12	9.18	9.24	9.30	9.36	9.43	9.49	9.55	9.62	9.68
20	8.97	9.00	9.06	9.12	9.18	9.24	9.30	9.36	9.42	9.48
21	8.76	8.82	8.88	8.94	9.00	9.06	9.12	9.18	9.24	9.30
22	8.59	8.65	8.71	8.77	8.83	8.89	8.95	9.01	9.07	9.13
23	8.43	8.48	8.54	8.61	8.66	8.72	8.78	8.84	8.90	8.96
24	8.28	8.33	8.39	8.45	8.50	8.56	8.62	8.68	8.73	8.79
25	8.13	8.18	8.24	8.29	8.35	8.41	8.46	8.52	8.57	8.63
	750	755	760	765	770	775	780	785	790	795
26	7.99	8.04	8.09	8.15	8.20	8.26	8.31	8.37	8.42	8.48
27	7.84	7.89	7.95	8.00	8.06	8.11	8.17	8.22	8.27	8.33
28	7.70	7.76	7.81	7.86	7.92	7.97	8.02	8.08	8.13	8.18
29	7.57	7.63	7.68	7.73	7.78	7.84	7.89	7.94	7.99	8.05
30	7.44	7.50	7.55	7.60	7.66	7.70	7.76	7.81	7.86	7.91
31	7.32	7.37	7.43	7.47	7.53	7.58	7.63	7.68	7.73	7.78
32	7.20	7.25	7.30	7.35	7.40	7.45	7.51	7.55	7.60	7.65
33	7.09	7.13	7.18	7.23	7.28	7.33	7.38	7.43	7.48	7.53
34	6.97	7.02	7.07	7.11	7.16	7.21	7.26	7.31	7.36	7.41
35	6.86	6.90	6.95	7.00	7.05	7.10	7.15	7.19	7.24	7.29
36	6.75	6.79	6.84	6.89	6.94	6.98	7.03	7.08	7.13	7.18
37	6.64	6.69	6.73	6.78	6.83	6.87	6.92	6.97	7.02	7.06
38	6.54	6.58	6.63	6.67	6.72	6.77	6.81	6.86	6.91	6.95
39	6.43	6.48	6.52	6.57	6.61	6.66	6.71	6.75	6.80	6.84
40	6.33	6.37	6.42	6.46	6.51	6.55	6.60	6.65	6.70	6.74
41	6.23	6.28	6.32	6.37	6.41	6.46	6.50	6.55	6.59	6.64
42	6.13	6.18	6.22	6.27	6.31	6.36	6.40	6.45	6.49	6.53
43	6.03	6.08	6.13	6.17	6.21	6.26	6.30	6.35	6.39	6.43
44	5.94	5.98	6.03	6.07	6.12	6.16	6.20	6.25	6.29	6.34
45	5.84	5.89	5.93	5.98	6.02	6.06	6.11	6.15	6.19	6.24
46	5.75	5.80	5.84	5.88	5.93	5.97	6.01	6.06	6.10	6.14
47	5.67	5.71	5.75	5.79	5.84	5.88	5.92	5.97	6.01	6.05
48	5.57	5.62	5.66	5.70	5.74	5.79	5.83	5.87	5.92	5.96
49	5.49	5.53	5.57	5.61	5.66	5.70	5.74	5.78	5.83	5.87
50	5.41	5.45	5.49	5.53	5.57	5.61	5.66	5.70	5.74	5.78

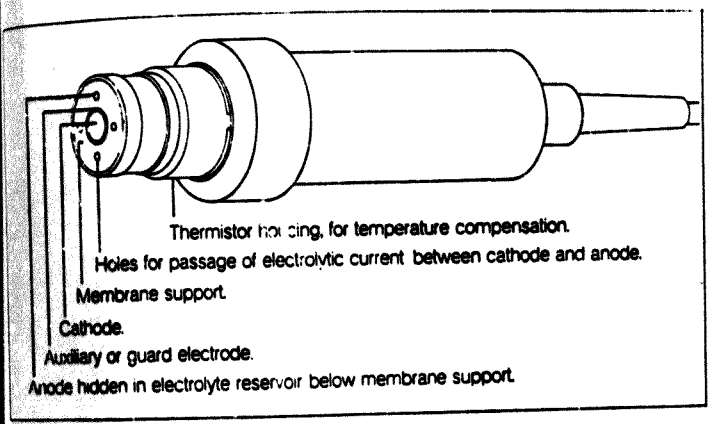

FIGURE 3.12: Perspective view of oxygen sensor

3.3.3 Flame Emission Techniques for Boron and Lithium Determinations

Atomic spectroscopy, which has been extensively applied to qualitative and quantitative analysis, is based on either absorption or emission of X-ray, ultraviolet, or visible radiation. X-ray emission or absorption involves excitation of those electrons that are closest to the nucleus and thus not involved in bonding (except for a few of the lightest elements). As a consequence, X-ray atomic spectra are produced regardless of the state of combination of the elements in the sample. Thus, the X-ray spectrum for nickel will be the same in solid nickel oxide, a solution of nickel (II) chloride, gaseous nickel carbonyl, or the elemental state. In contrast,

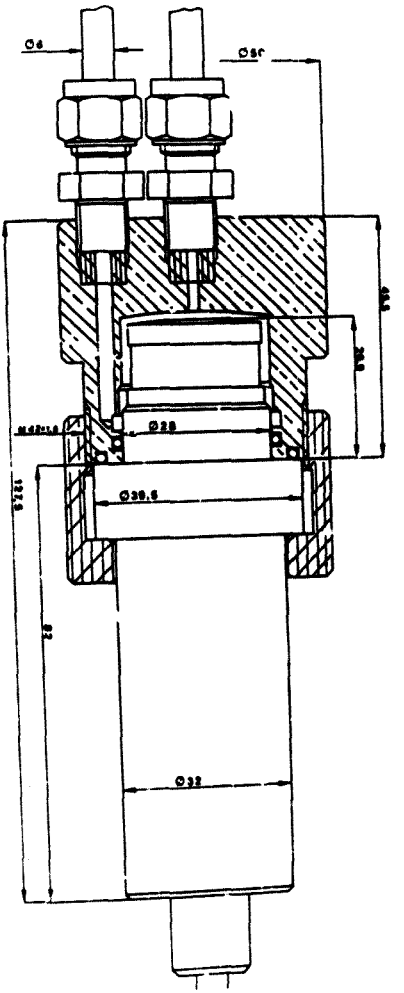

FIGURE 3.13: Sensor and flow chamber (dimensions in mm)

production of atomic spectra in the ultraviolet or visible regions requires conversion of the elements in a sample to gaseous monatomic particles (atoms or ions) because absorption or emission in these regions involves excitation of the outermost bonding electrons. Only by separat' an element from those to which it is bonded can pure atomic spectra be obtained.

Atomic spectra in the ultraviolet or visible region are produced by atomization of the sample, a process whereby the constituent molecules are decomposed and converted to gaseous elementary particles. Both the emission and the absorption spectrum of an atomized element consists of a relatively few discrete lines at wavelengths that are characteristic of the element.

The temperature of a flame is sufficient to excite a small fraction of the monatomic particles to higher electronic states. Their return to the ground state is accompanied by the production of emission lines, which can serve as a basis for flame-emission spectroscopy. Here the location of the lines provides qualitative information and their intensity permits quantitative analyses.

Flame-emission spectroscopy (also called flame photome' y) has found widespread application to elemental analysis. The most important applications have been to the analysis of sodium, potassium, lithium and calcium. For reasons of convenience, speed, and relative freedom from interference, flame-emission spectroscopy has become the method of choice for these otherwise difficult to determine elements.

Boron:

The highest sensitivity and best deflection-to-background ratio is given by an acetylene-air flame, using the acetylene burner. The flame must be a pure blue so as to keep the background as small as possible. Boron, in contrast to most other elements, has no strong

line that can be used for emission spectral analysis, but the BO_2 system of bands between 450 and 600 μm is sufficiently sensitive. Figure 3.14 gives a typical BO_2 band spectrum (useful range). Table 3.4 gives the corresponding sensitivities.

The bands have no self-absorption, so that the calibration graphs are always linear for pure boron solutions.

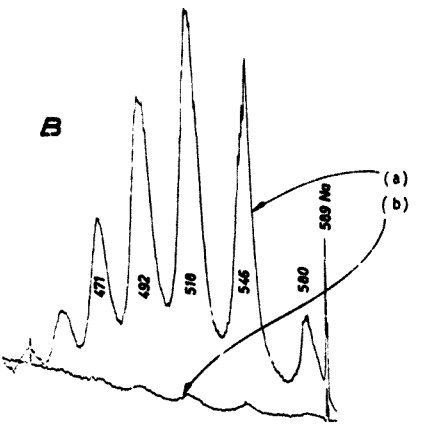

FIGURE 3.14: Typical spectra of BO_2 bands (a) 5 g B/litre; (b) 100 mg B/litre. Record at the same instrument setting.

TABLE 3.4: Sensitivities for the various monochromator settings

Monochromator setting (μm)	Sensitivity (%)
518	100
546	73
492	72
471	39
580	27

Lithium:

The highest sensitivity at the lowest background is given by a pure acetylene-air flame. To avoid spectral interferences and to keep the background as low as possible, narrow band widths are required during testing. Up to about 1 ppm there is no self-absorption and the calibration curves are linear.

The resonance lines at 670.8 µm and 323.26 µm are at a good distance from interfering lines so that relatively wide bands can be used:

wavelength	670.8 µm	323.3 µm
relative sensitivity	100%	0.6%
band width	1.0 µm	0.3 µm

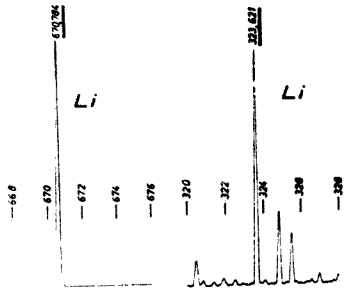

FIGURE 3.15: Line spectrum of lithium

3.3.4 Ion-Selective Measurement (pH, Cl^-, F^-)

The characteristics of most commercially produced pH electrodes are clearly defined and reproducible. The parameters are usually:

1. Zero point (E_0) - the pH value at which the electrodes (glass and reference) give an output of zero millivolts.

2. Isothermal intersection point (iso potential) - the pH value at which changes in temperature have minimal effect on electrode output.

3. Slope or sensitivity - the change in mV output per change (unit) in pH.

4. Resistance - the internal resistance of the electrodes considered as an e.m.f. generating cell.

Although the performance of ion-selective electrodes can be defined using the same parameters as those used for pH electrodes the values may vary much more widely. In step with the improvements in electrodes and meters, a fast growing body of ion-selective methodology has been formed. The ion-selective electrode responds to changes in activity in the ion being measured. In general concentration is of more interest. In many solutions activity and concentration are significantly different. Therefore, chemical pretreatment of the solution being measured is often required to maintain a constant ionic background for samples and calibrating standards. At present, there is a set of seven incremental methods, each possessing particular advantages and expanding the range of ion-selective applications. Recent developments in instrumentation have made these methods as straight forward to use as direct measurement.

The measuring system:

1. Ion-selective electrode (I.S.E.)
2. Reference electrode
3. High impedance voltmeter.

The I.S.E. senses the activity (and thus the related concentration) of the measured ion. The reference electrode provides a stable electrode potential and completes the electric circuit. The resultant potential difference is detected by the voltmeter and the concentration of the ion being measured is computed from the measured voltage.

The electrode characteristics are best shown by plotting a calibration or response curve. The electrode potential in mV is measured for a continuous range of ion activity solutions prepared from serial dilution of a pure standard solution. A typical response curve for a cation selective electrode is described in Fig. 3.16. There is a linear relationship between electrode potential and -log (activity) for most of the curve following the Nernst relationship:

$$E = E_0 + 2.303 \frac{RT}{zF} \log (a_{cation})$$

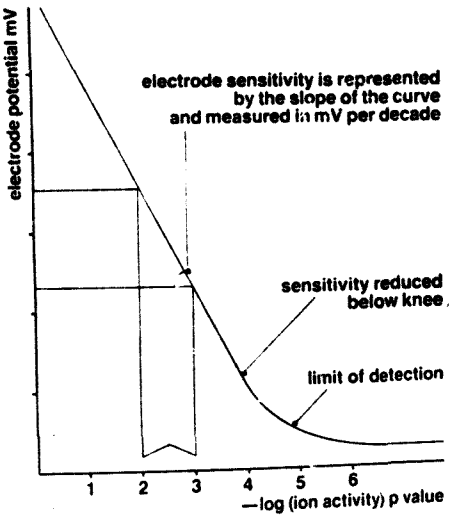

FIGURE 3.16: Typical response curve at 25 °C

Below the knee of the curve, the sensitivity of the electrode is reduced and is non-linear. This limit of detection governs the measuring range for each electrode. The factors affecting the overall response curve for all ion-selective electrodes are:

- Selectivity and Interferences
- Temperature
- Age
- High Concentration
- Contamination.

Ion-selective potentiometry is used for quantitative measurements of ions in solution. It is essential to take adequate care in preparing the sample and choosing experimental conditions to ensure best results. The preferred conditions will vary from application to application. Two areas to be considered are sample decomposition and sample pretreatment. The first covers dissolution of the sample (if required) and the second the treatment of the solution to simplify or improve the measurement technique.

Methods of Measurement:

There are three main methods of measurement with ion selective electrodes:

1. Direct potentiometry;
2. Incremental methods including sample and standard addition/subtraction and multiple additions or Grans Plot;
3. Potentiometric titrations.

The choice of method depends on the application and the kind of information needed. The following factors need to be considered

a) Activity or concentration required;
b) Condition of sample, complexed or free ion;
c) Accuracy of measurement;
d) Volume of sample available;
e) Time available for analysis,
f) Experimental conditions including temperature variation.

The direct potentiometric method is by far the most commonly used technique. However, the incremental methods are becoming increasingly important.

PW 9416 Ion-selective analyser: (Plate 3.11)

The Philips PW 9416 ion-selective analyser provides all the functions required for ion-selective analysis and provides them in a manner which is easily used by those inexperienced in the technique. Calibration and measuring methods are outlined step by step on a visual display unit in plain language. Input data is requested in an easily followed logical sequence.

PLATE 3.11: Ion selective analyser and electrode assembly

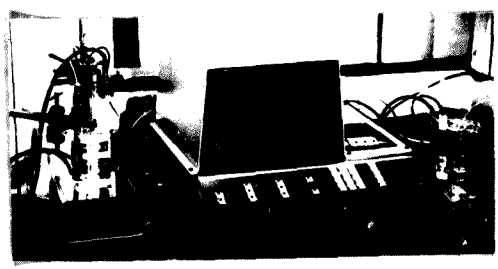

The display continuously shows the sensor output (including platinum resistance thermometer if used) and as each selection is made from the calibration and measurement method lists, it appears as a permanent reminder on the screen. Eight measurement modes are provided as well as direct concentration, sample addition/subtraction and standard addition/subtraction. There is dry sample addition/

subtraction, which allows direct addition of weighed solid or semi solid sample, eliminating the need to make sample solutions and providing direct results in % w/w of solid material.

The PW 9416 Ion-selective Analyser can also be used for the most accurate incremental method of all: Grans Plot. The Grans Plot result is automatically calculated from up to 8 readings and the 'goodness of fit' of the straight line plot indicated. Automatic calculations and display, mean that this method can be carried out in nearly the same time as single addition methods.

As well as appearing on the screen, results can be printed out on the built-in printer. Printer format can be selected so that main parameters can be printed out as well. If required, mean and standard deviation can be provided with each final result; thus reproducibility and accuracy of any group of results is easily checked. Two analogue recorder outputs are provided.

Once the sensor has been calibrated, the measurement parameters can be stored in permanent memory. Nine memories are available which are retained even if the instrument is turned off. When the data is required it can be entered (or edited and entered) into the operating memory and measurement commenced immediately.

Ranges:	pX:	- 1.0 .... 13.99
	mV:	-1999.9 .... 1999.9
	Concentration:	9.99 . . $10^{-13.99}$
	In selected units:	moles per litre mg per litre ppm µg per litre ppb µg %
	Temperature:	0.0 .... 99.9 °C
Resolution:	pX:	0.01
	mV:	0.1 mV
	Concentration:	1 digit in 9.99
	Temperature:	0.1 °C

The PW 9416 can be used for many ion determinations once the particular ion selective electrode has been purchased. The present electrodes include:

1. Combination pH electrode,
2. Pt-resistance thermocouple,
3. Chloride ion-selective electrode plus reference electrode,
4. Fluoride ion-selective electrode with reference electrode,
5. Ammonia gas combination electrode (used in high temperature P.W.R. tests when hydrazine dosing is required).

3.3.5 Dissolved Hydrogen Gas

Budget restrictions have dictated that hydrogen gas concentrations be estimated from published data. Unfortunately, conventional (non-nuclear) power stations that use Kent hydrogen analysers, have very low hydrogen levels. Therefore, all available instruments (that could be obtained through E.S.C.O.M.) would only be able to measure hydrogen concentrations at low levels (up to 200 ppb). Typical P.W.R. specifications include hydrogen concentrations of up to 50 ml/kg at S.T.P. (4 - 5 ppm).

Table 3.5 shows the solubility of hydrogen in water given the temperature and partial pressure of hydrogen in equilibrium with the water. The overpressures used in the experimentation will range from 0 - 40 kPa. Therefore, the hydrogen partial pressures, in equilibrium with the P.W.R. water will be 0 - 40 kPa plus atmospheric pressure (about 625 mm Hg).

TABLE 3.5: Solubility of hydrogen in water

T, °C	Solubility, cc./g, reduced to 0°C and 1 atm.								
	1 atm	25 atm	50 atm	75 atm	100 atm	300 atm	500 atm	700 atm	1000 atm.
0	0.0214	0.5363	1.068	1.601	2.130	6.139	9.83[illegible]	13.370	18.001
10	0.0193	0.4870	0.9690	1.435	1.932	5.579	8.980	12.214	16.623
20	0.0178	0.4498	0.8945	1.341	1.785	5.158	8.328	11.362	15.592
30	0.0163	0.4263	0.8475	1.271	1.689	4.897	7.922	10.818	14.928
50	0.0141	0.4067	0.8090	1.212	1.612	4.695	7.613	10.389	14.404
80	0.0085	0.4203	0.8385	1.254	1.667	4.866	7.885	10.757	14.867
100	0.0000	0.4615	0.9120	1.355	1.805	5.220	8.429	11.512	15.775

Knowing that test temperatures will be within the range of 20 - 80 °C, it can easily be calculated that dissolved hydrogen concentrations will be in the range:

T(°C)	Dissolved Hydrogen Range (std. cc/kg H_2O)
20	14.6 → 21.7
80	5.5 → 12.2

The P.W.R. specification for dissolved hydrogen is 0 - 50 std. cc/kg H_2O, so results are well within specification. The maximum overpressure of 40 kPa H_2 was chosen because of safety constraints on the Perspex cell and sealing system.

3.3.6 Sulphate Ion (SO_4^{2-}) Concentrations

As a result of the low sulphate concentrations expected in the rig water chemistry, ion-selective analysis would not be sensitive enough for sulphate determinations. Thus, sulphates would be determined via a titration technique ($BaCl_2$) after concentrating the solution using carefully controlled evaporation techniques. As a result of the delicate nature of such an evaporation technique, this work would be contracted out to Bergstrom and Bakker Analytical Laboratories.

3.3.7 Sample Potential Measurement

In order that actual P.W.R. conditions be best simulated, the corrosion fatigue specimens will not be isolated from the clevises during corrosion fatigue testing. Several experiments will be incorporated into the test programme to check the free corroding potential of the sample during the test. A saturated calomel electrode will be used as the reference electrode and an AMEL potentiostat (cell-out mode) will be used to measure the sample potential. The calomel electrode will be inserted into a Luggin probe which is inserted into one of the Perspex side covers to the test cell (see Plate 3.8 and Fig. 3.17). The probe will be positioned near to the

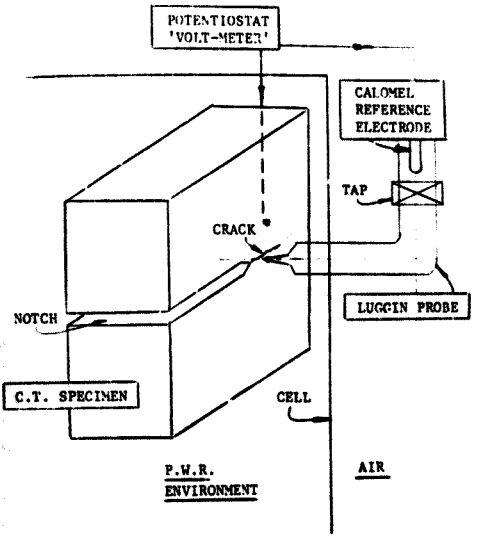

FIGURE 3.17: Sample potential monitoring set-up

start of the crack, but sufficiently far from the specimen so as not to disturb the local sample potential. The Luggin probe tap will be closed so as not to allow too much Cl^- ingress to the water but still provide an effective path for the conducting of ions. The 'voltmeter' will be connected to the sample via an electrical connector to the back of the C.T. specimen (approximately in front of the crack propagation direction).

3.4 SUMMARY

The corrosion fatigue test rig is designed to incorporate the maximum amount of flexibility in the final testing rig: the aim of the design is to provide simulated P.W.R. water so that C.F. testing could be carried out in recirculating P.W.R. water.

The facility includes tap water processing with filtration and deionization units. A microprocessor unit provides deoxygenated, low conductivity, demineralized water which is used as a water basis. Two stainless steel tanks are used for storage and make-up. The low T, P loop consists of diaphragm pumps for mixing and recirculatory flow, heater and heat exchanger for elevated temperature testing, in-line oxygen meter and sampling facilities, environmental test cell and finally a filter placed after the test cell to ensure that all particulate matter in the water is less than 0.2 μm.

Corrosion fatigue testing is carried out in a Perspex cell. The cell facilitates visual crack length measurements and potential drop leads for crack length measuring are also included. The fatigue testing is carried out on a 50 kN S.S.H. servo hydraulic testing machine and a waveform generator is incorporated for waveform generation. A Commodore Pet computer is used to generate waveforms for low frequency testing. The computer stores crack length data from the potential drop crack length monitoring system.

The potential drop crack length ing system relies on the following principle: A constant is passed through the Compact Tension specimen and as the propagates, so the potential difference across the crack changes. This difference corresponds to a crack growth increment.

Water chemistry is carefully controlled and monitored. Boron and lithium levels are increased to specified levels via boric acid and lithium hydr e dosing. Oxygen levels are reduced to specification via hy en purging. Table 3.6 gives the analytical techniques used fo emical analysis.

Sample potential monitoring can also be carried out, using an alternative side plate to the test cell that incorporates a Luggin probe with a Calomel electrode. Plates 3.12 3.14 show the entire test rig and related apparatus.

TABLE 3.6

Analysis	Analytical Techniques/Apparatus
Conductivity	Orion model 101 conductivity meter
Oxygen (Dissolved)	Orbisphere model 2713
Boron	Flame Emission
Lithium	Flame Emission
pH	Ion Selective Analysis
Chlorides (Cl^-)	Ion Selective Analysis
Fluorides (F^-)	Ion Selective Analysis
Hydrogen (Dissolved)	Saturation tables
Sulphates (SO_4^{2-})	$BaCA_2$ titration after sample concentration

PLATE 3.12: Water treatment, storage tank, in-line oxygen detector and diaphragm pumps

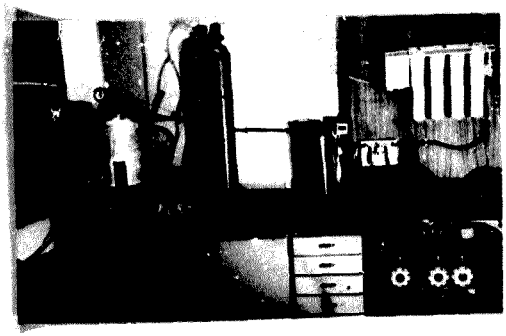

PLATE 3.13: Test cell, heater and heat exchanger, valve system for easy hydrog n purging of the cell.

PLATE 3.14: Micro computer, E.S.H. testing facility, test cell, constant current source and main rig in the background.

4.0 EXPERIMENTAL PROCEDURE

4.1 MATERIAL SPECIFICATION

The material used in this project was supplied to the Atomic Energy Commission by ESCOM. From discussions with ESCOM personnel, it was found that the steel sample was an off-cut generated during the manufacture of the Koeberg pressure vessel.

The pressure vessel sample was coded as follows:

CUVE K81
VIR B
CLEE 215 79
394 99

The block of steel had been cut into four sections. (Plates 4.1 to 4.4 show photographs of the 'assembled' block.) Note that the block is convex towards the outside wall dimension. It was assumed that the concave side faces towards the inside of the vessel.

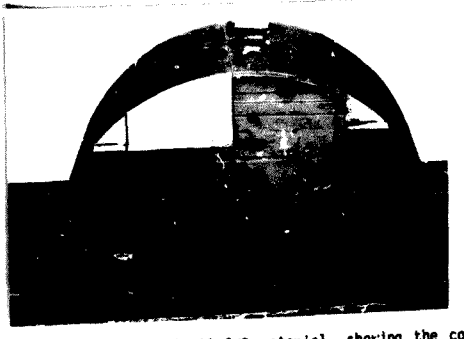

PLATE 4.1: Front view of SA508 C.3 material, showing the concave face. Regions were removed for chemical analysis.

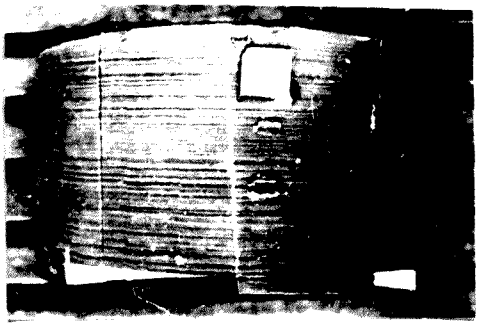

PLATE 4.2: Top view of the steel forging clearly showing the convex back face.

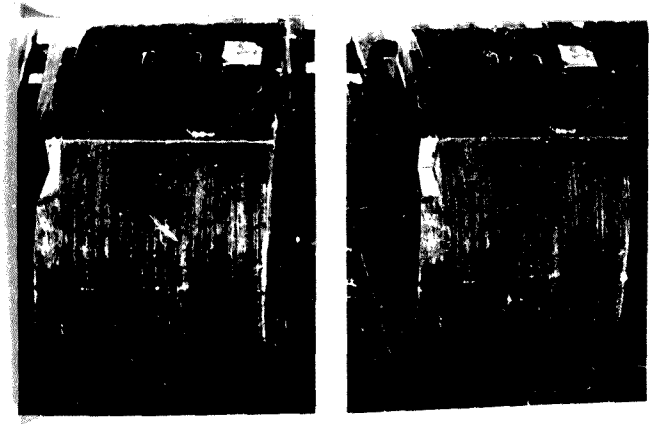

PLATES 4.3 and 4.4: Showing the convex and concave surfaces of the SA508 material respectively.

Figure 4.1 (a - d) shows a scaled sketch of the four sections of material. Block C was the only section used for obtaining specimens for mechanical and microstructural evaluation.

All corrosion fatigue specimens were machined so that the crack would grow in the through-thickness direction. Several specimens were also machined so that the crack growth direction would be normal to the through-thickness direction. Figure 4.2 shows block C with the C.T. specimen (Fig. 4.3) configurations.

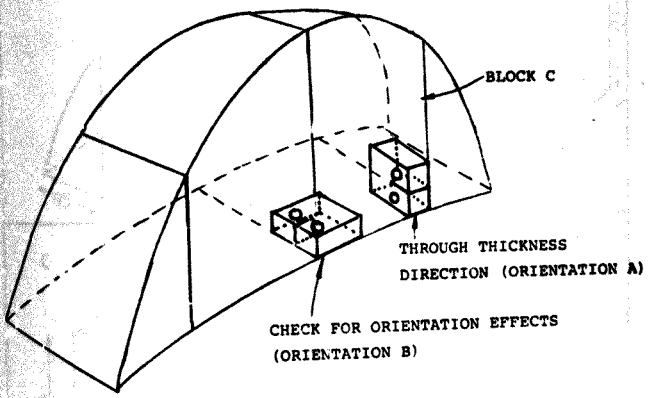

FIGURE 4.2: C.T. specimen orientations with respect to block C.

Several specimens were sent for chemical analysis. These included the sections shown in Plate 4.1 (already removed). Specimens were also taken from the front, back and mid-section of block C so as to check for through-thickness compositional variation.

4 SECTIONS HAVE BEEN CUT

COLOUR CODE :
face - red
base - green
back - yellow

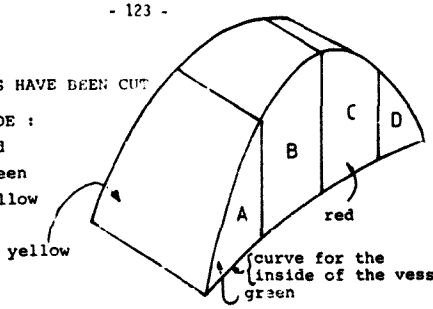

APPROXIMATE SECTION SIZES (mm).

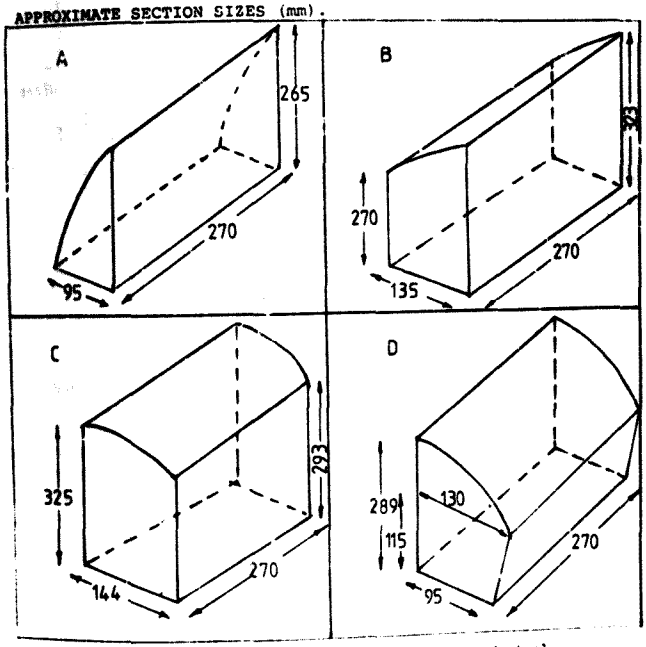

FIGURE 4.1:(A - D) Material: SA508 Cl3 forged steel.

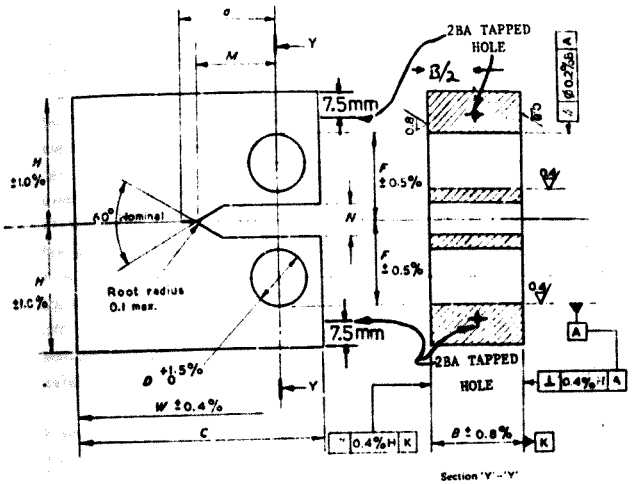

Net width W		
Total width C	=	1.25 W min.
Thickness B	=	0.5 W
Half height H	=	0.6 W
Hole diameter D	=	0.25 W
Half distance between hole outer edges F	=	1.6 D
Notch width N	=	0.065 W max.
Effective notch length M	=	0.25 W
Effective crack length a	=	0.45 W to 0.55 W

Test piece dimension	25 mm = B
D	$12.5^{+0.2}_{-0}$
F	20.0±0.10
N	3.25 max.
M	12.5
C	62.5 min.
W	50.0±0.20
B	25.0±0.20
H	30.0±0.30

All dimensions are in millimetres.

FIGURE 4.3: Proportional dimensions and tolerances for tensile test pieces with current lead placings (BS 5447).

Sections of block C were macro etched in 20% boiling HCl solution to reveal flow lines and inclusion clusters. Several samples were prepared for microstructural examination and hardness testing. These samples were taken at various through-thickness positions and orientations.

The determination of the sulphide distributions was undertaken at the front, rear and mid-section. To obtain the sulphur prints the specimens were carefully cleaned to remove grease. Photographic paper was soaked in a 5 ml concentrated sulphuric acid, 100 ml distilled water solution. The ground specimen was then placed against the paper, excluding all air bubbles. After a four minute contact time the paper was removed and fixed in a neutral fixing bath. The sulphur-containing inclusions, affected by the sulphuric acid, give off hydrogen sulphide which transforms the silver halide in the photographic emulsion to dark silver sulphide. By this means the sulphur distribution in the specimen is revealed.

Five Charpy specimens were machined in each of the orientations A and B. The Charpy specimens machined from orientation A producing crack growth directions analogous to the crack growth in the C.T. specimens marked orientation B. Five tensile specimens were also machined from block C in both orientations A and B.

All of the above tests were carried out to identify orientation effects, characterize the SA508 C.3 material and compare results with the ASTM specification for SA508 type material. The Framatome (manufacturing company) specification would also need to be referenced to confirm whether the pressure vessel steel conformed to mechanical property and heat treatment specifications.

4.2 CORROSION FATIGUE TEST PROGRAMME

The main section of this project involved corrosion-fatigue testing in simulated P.W.R. environments.

Sections of block C were macro etched in 20% boiling HCℓ solution to reveal flow lines and inclusion clusters. Several samples were prepared for microstructural examination and hardness testing. These samples were taken at various through-thickness positions and orientations.

The determination of the sulphide distributions was undertaken at the front, rear and mid-section. To obtain the sulphur prints the specimens were carefully cleaned to remove grease. Photographic paper was soaked in a 5 mℓ concentrated sulphuric acid, 100 mℓ distilled water solution. The ground specimen was then placed against the paper, excluding all air bubbles. After a four minute contact time the paper was removed and fixed in a neutral fixing bath. The sulphur-containing inclusions, affected by the sulphuric acid, give off hydrogen sulphide which transforms the silver halide in the photographic emulsion to dark silver sulphide. By this means the sulphur distribution in the specimen is revealed.

Five Charpy specimens were machined in each of the orientations A and B. The Charpy specimens machined from orientation A producing crack growth directions analogous to the crack growth in the C.T. specimens marked orientation B. Five tensile specimens were also machined from block C in both orientations A and B.

All of the above tests were carried out to identify orientation effects, characterize the SA508 C.3 material and compare results with the ASTM specification for SA508 type material. The Framatome (manufacturing company) specification would also need to be referenced to confirm whether the pressure vessel steel conformed to mechanical property and heat treatment specifications.

4.2 CORROSION FATIGUE TEST PROGRAMME

The main section of this project involved corrosion-fatigue testing in simulated P.W.R. environments.

Several parameters were investigated and these included:

1) P.W.R. versus Air testing.

2) 0.2 R-ratio versus 0.7 R-ratio tests for both P.W.R. and air environments (at two frequencies).

3) Through-thickness crack growth directions versus crack growth normal to this direction. The effect of environment and frequency was investigated.

4) Effect of temperature variation: 50 °C versus 20 °C. Two frequencies were tested.

A detailed description of the testing programme is given in the table below. (Other work carried out in the Department included a detailed discussion of frequency effects (30 - 0.067 Hz) and waveform loading [49].)

4.2.1 Testing procedure

The 1 T C.T. (compact tension) specimens were prefatigued in air to a crack length (a) of approximately 18 mm. This corresponds to about 3 mm of fatigued crack growth. Sinusoidal waveform loading at a frequency of 40 Hz was used for prefatguing. The last millimetre of crack growth was always carried out at the R-ratio of the test to be performed, on the precracked specimen. This was necessary to reduce later transient effects resulting from plastic zone formation.

During testing, crack length measurement was made at discrete cycle intervals. The duration time for visual crack length determination was about 60 secs and when the test was being computer controlled, the time required to record the P.D. reading and process the data was approximately 5 secs. During these intervals the fatiguing was halted. Clearly, to reduce the possibility of inducing any large plastic zone regions, the dwell time was kept as short as possible. (The test was stopped at the mean load.)

TABLE 4.1: Test description for corrosion fatigue tests

ıst	Environment	R-ratio	Frequency (Hz)	Waveform	Temperature (^{0}C)	Potential Monitoring	Maximum Load	Through-thickness Crack Growth
(1)	AIR	0.2	10	Sinusoidal	20	-	25 kN	Yes
(2)	AIR	0.7	10	Sinusoidal	20	-	25 kN	Yes
(3)	AIR	0.2	1	Sinusoidal	20	-	25 kN	Yes
(40R)	AIR	0.2	10	Sinusoidal	20	-	25 kN	No
R. (1a)	P.W.R. water	0.2	10	Sinusoidal	20	No	25 kN	Yes
.R. (1b)	P.W.R. water	0.2	1	Sinusoidal	20	Yes	25 kN	Yes
.R. (2a)	P.W.R. water	0.2	10	Sinusoidal	20	Yes	25 kN	No
.R. (2b)	P.W.R. water	0.2	1	Sinusoidal	20	Yes	25 kN	No
.R. (3a)	P.W.R. water	0.2	10	Sinusoidal	50	Yes	25 kN	Yes
I.R. (3b)	P.W.R. water	0.2	1	Sinusoidal	50	Yes	25 kN	Yes
W.R. (4a)	P.W.R. water	0.7	10	Sinusoidal	20	No	25 kN	Yes
W.R. (4b)	P.W.R. water	0.7	1	Sinusoidal	20	No	25 kN	Yes

Visual crack length measurment was aided by the use of the travelling microscope (x10 magnification) having a resolution of 0.01 mm. To aid in visually determining crack length, one side of the specimen was ground to a 1000 grit surface finish.

Initial 'dummy' specimens were produced to account for crack curvature. Several tests were conducted at various R-ratios, keeping P_{max} (maximum load) constant, and beach marking was used to differentiate these R-ratio regions. A seven point, through-thickness (average) crack length was used to correlate the actual recording made during the test. This is termed the correction for crack curvature and all visual crack length measurements are adjusted accordingly.

To calibrate the potential drop (P.D.) crack length monitoring unit, potential difference readings are taken for various crack growth increments. The potential values are then related to crack length using Johnson's equation [49]. Johnson's equation was found consistently to underestimate the crack length, especially during the final stages of crack growth. The crack length results were therefore adjusted, using the data obtained from the crack curvature determinations (a simple linear regression was used).

Computer facilities assisted in the control of the fatigue tests. The facility was prompted with the specimen identification and dimensions, load, p.d. probe spacing, test frequency, initial crack length and test stopping criterion. Discrete cycle intervals were used for prompting the computer to 'receive' potential difference readings. These were then converted to crack length using Johnson's equation. Cycles, computed crack length and voltage were then printed out and stored on disk. This data was only later corrected to give 'true' crack length.

For tests performed at 10 Hz the waveform was generated via a function generator, but for lower frequencies the waveforms had to be compiled analytically, since the system could not pass the required signal from the function generator to the computer. This is simply

an interfacing problem. When the desired number of cycles has accrued, fatiguing is momentarily halted and the Fluke voltmeter is activated. Five potential difference readings are taken and the highest reading is retained and converted into crack length. This value is compared to the stopping criterion and if the stopping criterion has not yet been met, the fatiguing process is continued.

4.2.2 **Data Reduction** (using BS 5447 and ASTM 399 standards)

The 'true' crack length (a) corresponding to a number of fatigue cycles (N) is converted into crack growth rate (da/dN) data as a function of ΔK, the stress intensity factor range. An incremental polynomial (7 point) method is used to smooth the a versus N data (ASTM 399) analytically. The data reduction programme therefore incorporates the capability of analysing the data and subsequently plots the da/dN versus ΔK graphs.

The stress intensity range is calculated using the smoothed a versus N data.

$$\Delta K = \frac{\Delta P}{BW^{1/2}} (Y)$$

where ΔP : fatigue load range = $P_{max} - P_{min}$

B : specimen thickness

W : specimen width

Y : compliance function given by the expression below (a is the 'true' smoothed crack length):

$$Y = 29.6\,(a/w)^{1/2} - 185.5\,(a/w)^{3/2} + 655.7\,(a/w)^{5/2} - 1017(a/w)^{7/2} + 638.9\,(a/w)^{9/2}.$$

The final result is therefore a curve of da/dN versus ΔK for the test.

4.2.3 **Scanning Electron Microscopy** (S.E.M.)

All fatigue fracture surfaces were examined under the S.E.M. with an EDAX facility also being used. This involved the removal of the

fracture surface from the C.T. specimen. Two specimens were observed under the S.E.M. after ultrasonically cleaning the fracture surfaces. It was, however, found that machining the fracture surface from the C.T. specimen left extraneous material on parts of the fracture surface. Also, preparation for S.E.M. studies was often carried out long after the completion of the corrosion fatigue test. This meant that the samples were only fractured open at a later stage. In order to create a clean fracture surface all S.E.M. samples were subsequently given a cathodic treatment.

The cathodic treatment (using the Endox process) is as follows:

1. NaOH (123 g) is mixed with 1000 ml of cold water, in a fume-cupboard.

2. When the temperature is below 50 °C, 86 g of NaCN is added to the NaOH solution.

3. The specimen (acting as the cathode) is then inserted into the solution and a voltage of 6 - 9 V was applied. A platinum electrode acted as the anode (working electrode). Profuse hydrogen evolution from the specimen surface removes light oxide scale and the more adherent oxide is reduced without damaging fractographic features.

4. After several minutes of this cathodic cleaning, the specimen is placed in a 5% NH_3 solution in an ultrasonic bath for several minutes.

5. The material is then ultrasonically cleaned in ethanol and blown dry.

Although this process is usually used to remove scale from the high temperature (288 °C) corrosion fatigue test specimens it has proved to be a useful cleaning technique of fractographic surfaces, in general.

4.2.4 Sample Potential Monitoring

Figure 3.17 shows the experimental rig for sample potential monitoring. The 'mouth' of the Luggin probe is approximately 1 cm from the side face of the C.T. specimen, corresponding to the point of crack initiation. At regular intervals the tap on the Luggin probe was opened to create an electrical path between the specimen and the reference electrode (S.C.E.). The tap was closed after obtaining a potential reading so that chloride ingress to the P.W.R. water was insignificant. After each test the Luggin probe was opened and the cell water was then purged to drain. Potential monitoring tests were carried out on specimens P.W.R. (1b), (2a), (2b), (3a) and 3(b).

To correlate the results from the potential monitoring tests, potentiodynamic tests (to determine E_{corr}) were carried out for SA508 C.l3 at the two temperatures of interest (20 and 50 °C). The tests involved purging hydrogen through a potentiostatic test cell that had been filled with P.W.R. simulated water (±1 ℓ). One hour stabilization period was allowed before E_{corr} was determined [50]. For one of the tests SA508 C.l3 (20 °C) a potentiodynamic scan was performed to check the performance of SA508 C.l3 steel in a P.W.R. environment. A sample of AISI type 316 stainless steel was also tested to determine E_{corr} in the P.W.R. environment. 316 stainless steel was used to manufacture the clevis arrangement and it was therefore necessary to correlate the potentials of SA508 C.l3 and AISI type 316 stainless steel when in electrical isolation. No electrical isolation was employed during fatigue testing.

4.2.5 Water Chemistry Control

Prior to filling the system with P.W.R. type water the rig was assembled and cleaned. Initially tap water was pumped through the system. This was followed by a alkaline wash with a degreasing agent (mild alkaline solutic at pH = 8 - 9). The rig was then rewashed several times with tap water and finally with ultrapure

water. The system was kept under hydrogen pressure until the storage tank was filled with the ultrapure demineralized/deoxygenated water. Lithium hydroxide and boric acid additions were made through the dosing lock nut in the top of the tank. The dosed water was then pump-mixed while continuously bubbling hydrogen through the storage tank. After approximately four hours the oxygen concentration was reduced to specification (i.e. O_2 <100 ppb ; Typically O_2 <10 ppb).

Daily checks were initially carried out to check that the water chemistry conformed to P.W.R. specifications (see table below).

TABLE 4.2: P.W.R. Water Chemistry Specification.

Conductivity (inlet) $\mu S.cm^{-1}$	1 - 40
Oxygen (ppb)	<100
Hydrogen, mℓ/kg at S.T.P.	0 - 50
LiOH, ppm	0.6 - 6.2
H_3BO_3, ppm	0 - 13000
Cl^- ppm	<0.15
F^- ppm	<0.15
pH (25 °C)	4.0 - 10.5

It was found that the water specification remained constant for long periods of time. Only after several months did the chloride level rise to above specification levels. The water was then replaced with a new batch of water and subsequently dosed (B and Li) to specification.

Before each corrosion fatigue test (after prefatiguing in air), the test cell side plates were fastened to the cell and hydrogen was purged through the test cell, only. As the main storage tank was kept under approximately 30 kPa H_2 over-pressure the test cell could be easily filled without starting the recirculating pump. The gradual filling of the cell prevented the entrapment of hydrogen bubbles in the C.T. specimen notch. The diaphragm pump stroking distance was then increased until a flowrate of 26 ℓ/hr was ob-

tained. The corrosion fatigue test was then started. The sampling point for chemical analysis was situated just before the recirculating pump. It was at this point that the oxygen meter was placed in a flow-through sampling unit.

On completing a test, the cell was emptied of water by forcing the P.W.R. water back into the storage tank with the use of hydrogen pressure. The H_2 pressure in the cell was then relieved once the unit had been isolated from the recirculating loop. The hydrogen pressure was relieved by opening a ball valve. At this point the cover plates and specimen could be removed.

Several water samples were sent to specialist analytical organizations for Cl^-, F^- and SO_4^{2-} analyses and every sample was analysed, for Ca^{++}, F^-, B, Li, pH and conductivity determinations, in the Corrosion Laboratory at the University of the Witwatersrand.

4.3 SUMMARY

A forged section of SA508 C.3 steel, from a nozzle section, was used for microstructural and mechanical testing of Koeberg nuclear reactor. Microstructural studies included optical microscopy, macroscopy, sulphur printing and scanning electron microscopy of the corrosion fatigue fracture surfaces. The mechanical testing included Charpy Impact tests, tensile tests, Vickers pyramid hardness testing and corrosion fatigue testing. Sample potential monitoring was carried out for several of the corrosion fatigue tests carried out in P.W.R. environments. This work was later correlated to potentiodynamic polarization tests.

The corrosion fatigue testing included tests aimed to check the effects of environment (P.W.R. versus air tests), orientation (through-thickness versus normal to through-thickness crack growth), temperature (20 °C versus 50 °C), R-ratio (0.7 versus 0.2) and frequency (10 Hz versus 1 Hz). Orientation effects were checked for all of the mechanical and microstructural tests.

A large part of the experimental procedure involved the setting up of a flow-through system to simulate P.W.R. water environments within the corrosion fatigue test cell, the main aim being that the water should comply to P.W.R. and I.C.C.G.R. standard specifications.

5.0 RESULTS

The results can be divided into three subsections:

5.1 General mechanical testing and microscopy.

5.2 Corrosion fatigue tests with the related scanning electron microscopy of the corrosion fatigue fracture surfaces.

5.3 Potential monitoring during corrosion fatigue testing and related potentiodynamic studies.

5.1 MATERIAL PROPERTIES

5.1.1 Charpy Impact Tests

For the Charpy specimens machined along orientation A (i.e. crack propagation normal to the through-thickness direction) the following results were obtained:

TABLE 5.1: Charpy Impact Energy in Joules

Temperature = 20 °C	
Sample	Charpy Impact Energy Joules (J)
1	158
2	186
3	160
4	134
5	134

Therefore the average Charpy impact toughness is 154 J with a standard deviation of 21.7 J.

For crack propagation in the through-thickness direction, the five Charpy impact values were as follows:

5.0 RESULTS

The results can be divided into three subsections:

5.1 General mechanical testing and microscopy.

5.2 Corrosion fatigue tests with the related scanning electron microscopy of the corrosion fatigue fracture surfaces.

5.3 Potential monitoring during corrosion fatigue testing and related potentiodynamic studies.

5.1 MATERIAL PROPERTIES

5.1.1 Charpy Impact Tests

For the Charpy specimens machined along orientation A (i.e. crack propagation normal to the through-thickness direction) the following results were obtained:

TABLE 5.1: Charpy Impact Energy in Joules

Temperature = 20 °C	
Sample	Charpy Impact Energy Joules (J)
1	158
2	186
3	160
4	134
5	134

Therefore the average Charpy impact toughness is 154 J with a standard deviation of 21.7 J.

For crack propagation in the through-thickness direction, the five Charpy impact values were as follows:

TABLE 5.2: Charpy impact values for through-thickness crack growth

Temperature = 20 °C	
Specimen	Charpy Impact Energy Joules (J)
1	272
2	300
3	284
4	244
5	242

The average Charpy Impact Energy is therefore 268 J with a standard deviation of 25 J.

5.1.2 Tensile Tests

For the five Hounsfield tensile specimens, in each of orientations A and B, the tensile test gave no indication of an orientation effect. The results are presented in Table 5.3. The testing conditions were:

- Room temperature testing = 20 °C
- Strain rate = 3×10^{-2} mm/sec.
- Specimen configuration ℓ_0 = 23.00 mm
  dia_0 = 5 mm

TABLE 5.3: Tensile Test Results for both Orientation A and B

Specimen Orientation	Yield Stress σ_Y (MPa)	Tensile Stress $\sigma_{U.T.S.}$ (MPa)	Elongation (%)	Reduction in Area (%)
A1	490.5	621.9	22.98	64.00
A2	490.1	621.5	21.39	65.89
A3	494.0	624.3	23.67	65.43
A4	499.1	628.8	21.98	67.74
B1	494.0	633.2	22.08	72.96
B2	493.0	627.6	23.74	72.75
B3	492.5	624.9	23.66	72.12
B4	488.9	627.8	23.77	71.91
B5	490.9	622.3	22.57	69.53

The tensile property values are given below as an average (standard deviation):

Specimen Orientation	Yield Stress (MPa)	Tensile Stress (MPa)	Elongation (%)	Reduction in Area (%)
A	493.4 (4.19)	624.1 (3.34)	22.51 (1.02)	65.77 (1.54)
B	491.9 (1.99)	627.1 (4.05)	23.16 (0.79)	71.85 (1.37)
A and B	492.6 (3.03)	625.8 (3.86)	22.87 (0.90)	69.15 (3.48)

5.1.3 **V.P.N. Hardness Tests**

Figure 5.1 below shows the forged SA508 material.

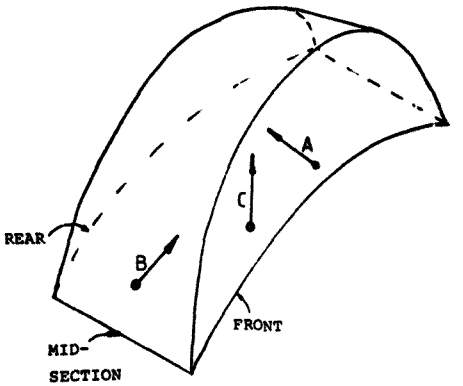

FIGURE 5.1: Forged SA508 steel block showing orientations A, B and C.

Hardness determinations were taken in all three orientations and the results presented below. The results (30 kg load) are an average of ten determinations.

TABLE 5.4: Hardness as a Function of Orientation

Orientation	Hardness (VPN)
A	225
B	235
C	220
Average	227

As with the tensile tests, little orientation effect was noticed. The hardness determinations were carried out along the thickness of steel block and no through-thickness variations were noted.

5.1.4 Chemical Analysis

The following table represents chemical analyses from 10 determinations. Included are chemical analyses from front, mid and rear sections of the SA508 forged material (block C). An average is quoted for all of the chemical analyses, which also include sample analyses from other sections i.e. block A and B.

TABLE 5.5 Chemical analyses presented as an average of at least 5 determinations. The final column is an average of 25 chemical analyses.

Element	Front section (wt%)	Mid Section (wt%)	Rear Section (wt%)	Average (wt%)
C	0.15	0.16	0.16	0.16
Mn	1.29	1.32	1.33	1.38
P	0.014	0.010	0.011	0.013
S	0.008	0.007	0.006	0.008
Si	0.25	0.24	0.24	0.25
Ni	0.74	0.74	0.75	0.77
Cu	0.05	0.06	0.06	0.06
Cr	0.24	0.25	0.25	0.26
Mo	0.48	0.49	0.50	0.52
V	0.016	0.012	0.012	0.013
Al	0.029	0.031	0.031	0.029
Sn	0.016	0.016	0.016	0.016
Co	0.029	0.024	0.022	0.021

5.1.5 Optical Microscopy

Metallographic samples were prepared from each of orientations A, B and C (Fig. 5.1) and samples were chosen so that through-thickness variations could also be examined.

Results showed that no through-thickness effects were visible but, that there was evidence of banding. Plate 5.1 shows the general microstructure which corresponds to the expected bainitic microstructure for this steel. Plate 5.2 shows quite clearly the alternating bands of dark (segregated) and light upper bainite. These bands clearly correspond to the working direction of the forged billet.

PLATE 5.1: General bainitic microstructure

SCALE: ⟵⟶ = 200 μm

PLATE 5.2: Dark and light bainitic bands corresponding to the working direction. This is a normal segregation effect in wrought products

SCALE: ⟵⟶ = 50 μm

Long stringer type manganese sulphides were clearly visible in some of the metallographic specimens. These sulphides were, however, only observed in the dark etching bainite (see Plates 5.3 - 5.5).

PLATE 5.3: MnS stringer in dark bainitic structure

SCALE: ⟷ = 50 μm

Note that plate 5.5. still shows prior austenitic grain boundaries.

PLATE 5.4: MnS stringers and prior austenitic grain boundary visible

SCALE: ⟷ = 100 μm

PLATE 5.5: Sulpnide stringers and prior austenitic grain boundaries (triple point) clearly visible

SCALE: ⟵⟶ = 50 μm

50 μm grain size corresponds to an ASTM grain size No. of 6.

From approximately 20 microstructural investigations it was learnt that the dark bainitic bands lie in the orientations shown below (Fig. 5.2). The sulphide stringer network directions are also shown. This corresponds to the direction of grain flow. Figure 5.3 represents a plan and side view of the forging.

6.1.6 Macroscopy and sulphur prints

Sulphur prints were made from various sections of the block C, primarily to determine the sulphide orientations and secondly to determine the 'cleanliness' of the steel. The results of the investigation simply 'amplified' the findings from microstructural observations. Large sections of the SA508 material were also etched in a boiling 20% HCl solution. Regions of the steel were 'etched-out' and these regions corresponded to the regions of sulphide inclusions.

PLATE 5.5: Sulphide stringers and prior austenitic grain boundaries (triple point) clearly visible

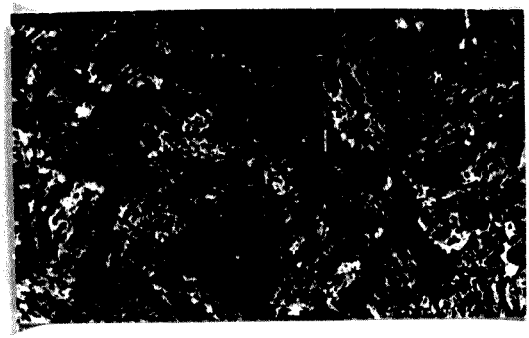

SCALE: ⟷ = 50 μm

50 μm grain size corresponds to an ASTM grain size No. of 6.

From approximately 20 microstructural investigations it was learnt that the dark bainitic bands lie in the orientations shown below (Fig. 5.2). The sulphide stringer network directions are also shown. This corresponds to the direction of grain flow. Figure 5.3 represents a plan and side view of the forging.

5.1.6 Macroscopy and sulphur prints

Sulphur prints were made from various sections of the block C, primarily to determine the sulphide orientations and secondly to determine the 'cleanliness' of the steel. The results of the investigation simply 'amplified' the findings from microstructural observations. Large sections of the SA508 material were also etched in a boiling 20% HCl solution. Regions of the steel were 'etched-out' and these regions corresponded to the regions of sulphide inclusions.

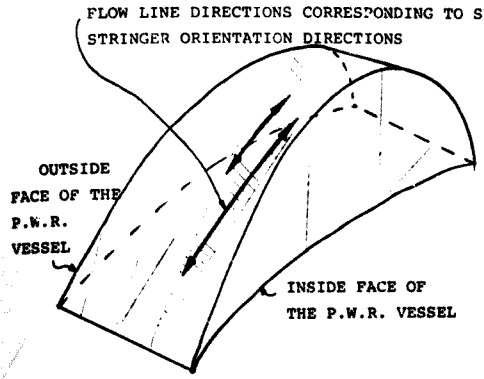

FIGURE 5.2: Flow lines and sulphide stringer directions.

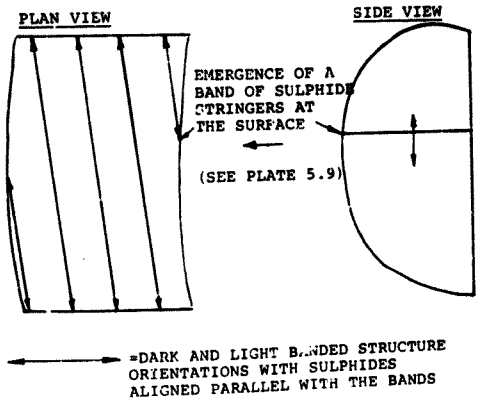

FIGURE 5.3: Plan and side view of SA508 forging showing sulphide and flow line orientations.

The following plates have been included and Fig. 5.4 shows the regions that were investigated.

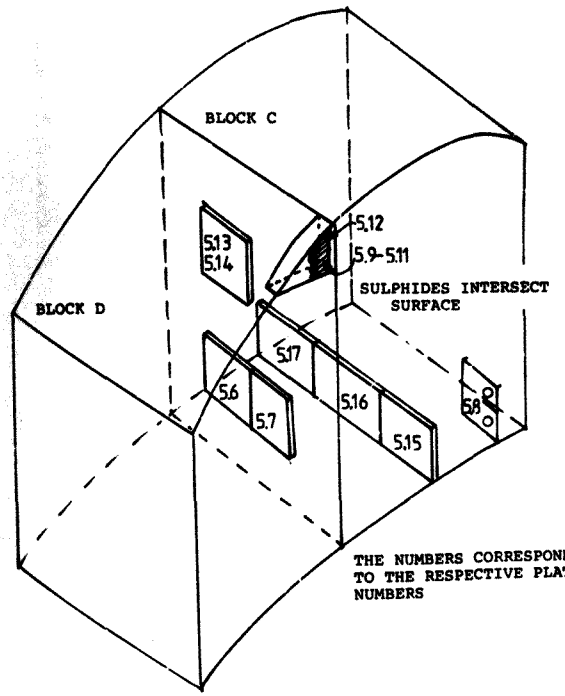

FIGURE 5.4: This figure corresponds to plates (5.6 - 5.17), showing the orientation of plate to the main block C.

PLATE 5.6: This sulphur print shows an edge-on view of the sulphide stringers. Note that the sulphides are clustered together. (Mag. 1 : 1)

PLATE 5.7: A cleaner section of steel but, still 'riddled' with sulphides (sulphur print). (Mag. 1 : 1)

PLATE 5.8: A C.T. specimen side-face showing a more uniform sulphide distribution. (Mag. x 1.3)

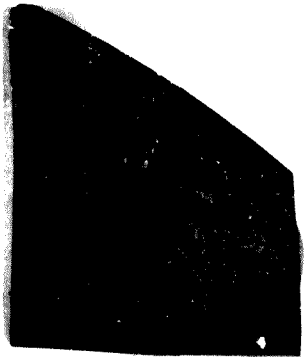

PLATE 5.9: Macro etched section (5 mins) showing flow lines and dark central region. (Mag. x 1)

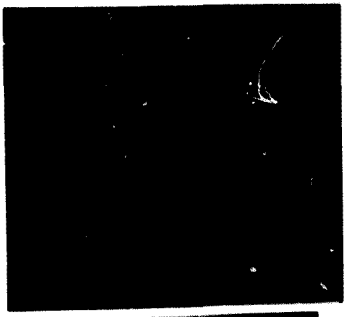

PLATE 5.10: Macro etch (20 mins). Deeply etched sulphide region. (Mag. x 1)

PLATE 5.11: Macro etch (2hrs) showing that sulphides are in fact stringers which have emerged at the inside surface wall. (Mag. x 3.2)

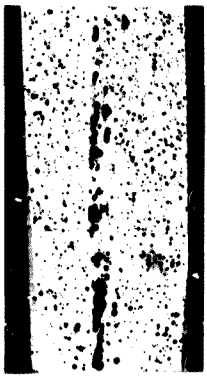

PLATE 5.12: Macro etch showing the sulphide stringer (clusters) which are a continuation of those observed in plates 5.9-5.11 (Mag. x 2)

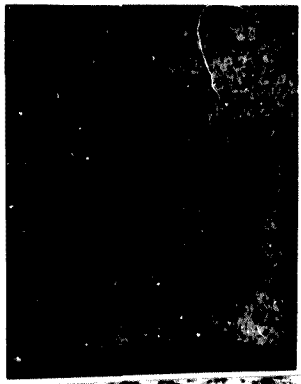

PLATE 5.13: Typical macro etched region (over etched to etch out the sulphides). (Mag. x 1)

PLATE 5.14: Magnified view (x2) of the 'black-boxed' region in plate 5.13. End on view of sulphide's location, clearly visible. Note the clustering of sulphides.

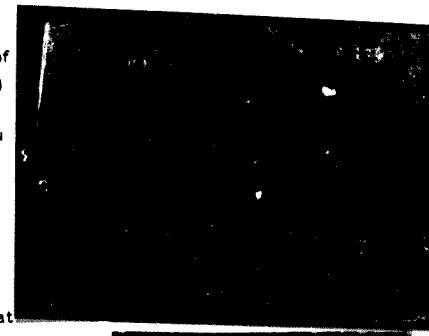

PLATE 5.15: Front section of block C showing a more densely (sulphide) popu lated inside surface (A). (Mag. x 1)

PLATE 5.15 - 5.1/: Show rough machined surfaces that have been etched in boiling 20% HCl. Machining has purposefully resulted ir scratches normal to ' sulphide stacking direction.

PLATE 5.16: Mid section, showing that large clusters of sulphides appear throughout the block of SA508 material. (Mag. 1.4)

PLATE 5.17: Outside section of block C. Once again showing a higher sulphide concentration at the block face (B). (Mag. x 1)

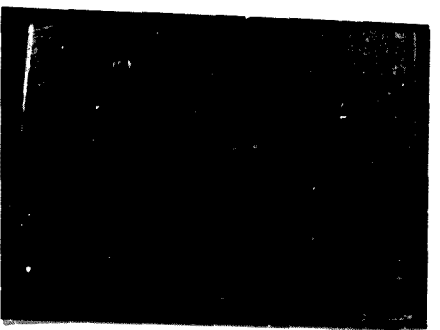

PLATE 5.15: Front section of block C showing a more densely (sulphide) popu lated inside surface (A). (Mag. x 1)

PLATE 5.15 - 5.17: Show rough machined surfaces that have been etched in boiling 20% HCl. Machining has purposefully resulted in scratches normal to the sulphide stacking direction.

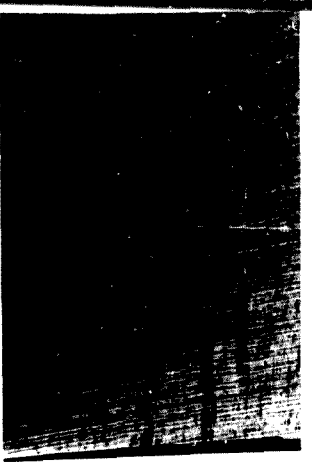

PLATE 5.16: Mid section, showing that large clusters of sulphides appear throughout the block of SA508 material. (Mag. 1.4)

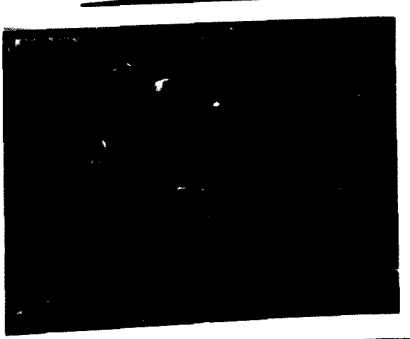

PLATE 5.17: Outside section of block C. Once again showing a higher sulphide concentration at the block face (B). (Mag. x 1)

5.2 Corrosion Fatigue Tests

This section deals with the crack growth behaviour as defined by the observed crack growth rate (da/dN) as a function of the applied cyclic stress intensity range (ΔK). Each test result will be presented separately and will include the fractographic features observed during scanning electron microscopy studies. After each set of results, various single da/dN versus ΔK curves will be combined to compare the effects of all the testing variables.

A detailed discussion of all the results will be included in the discussion section. On all the da/dN versus ΔK curves the ASME XI (1980) upper bound curves have been superimposed. These curves represented an upper limit on the crack growth rates in air and P.W.R. environments, at that time.

The fracture surface descriptions include discussions on ductile striated fracture surfaces.

The definition for the above term is given below.

Ductile Striations

1. Irregular striations.
2. Primary and secondary striations.
3. Deep striations.
4. Secondary cracking.
5. Lack of tear ridges in direction of crack propagation.
6. No fan shaped features.

Other fractographic features include environmentally assisted crack growth regions. These areas have resulted in fan shaped growth originating from inclusions.

All P.W.R. tests were carried out with a water chemistry analysis as shown in Table 5.6.

TABLE 5.6: Water Chemistry for P.W.R. Tests

Conductivity (K) (25 °C)	<25 μS
pH (25 °C)	6.5 ± 0.2
O_2 (25 °C)	<10 ppb
F^- (25 °C)	<40 ppb
Cl^- (25 °C)	<120 ppb
B (25 °C)	±900 ppm
Li (25 °C)	±1.6 ppm
H_2 saturation at 20 °C	5.5 - 21.7 std. cc/kgH_2O
SO_4^{2-}	<30 ppb

5.2.1 Air (1) and Air (3) tests

Figures 5.5 and 5.6 show the da/dN versus ΔK curves for tests AIR (1) and AIR (3). The two curves have been superimposed in Fig. 5.7 and it can be seen that decreasing the frequency of testing (in air) from 10 Hz to 1 Hz has had no effect on the crack growth rate of SA508 Cl3 steel. Clearly, both curves lie below the ASME XI (1980) crack growth rate curve for a subsurface flaw, tested in air.

As can be expected, both the air tests produced similar fracture surfaces. Plates 5.18 - 5.20 show the fracture mode to be ductile and only in certain regions have inclusions been observed. However, these inclusions have not interfered with the crack growth mechanism (i.e. no brittle - fast fracture regions about the inclusions). However, the crack growth would be affected by the presence of inclusions which would 'weaken' the matrix in the vicinity of the inclusion, since MnS is a non-coherent precipitate. The length of inclusion would lead one to assume that the inclusions are of Type II [51]. (Plate 5.21 shows an EDAX analysis of the inclusions.) Clearly they are MnS and indeed, all the inclusions found on the fracture surfaces (P W.R. environment tests as well) were identified as MnS.

In general, the two air test fracture surfaces were found to be quite clean (i.e. few MnS inclusions) and the MnS inclusions were found to lie normal to the crack growth direction.

TABLE 5.6: Water Chemistry for P.W.R. Tests

Conductivity (K) (25 °C)	<25 μS
pH (25 °C)	6.5 ± 0.2
O_2 (25 °C)	<10 ppb
F^- (25 °C)	<40 ppb
Cl^- (25 °C)	<120 ppb
B (25 °C)	±900 ppm
Li (25 °C)	±1.6 ppm
H_2 saturation at 20 °C	5.5 - 21.7 std. cc/kgH_2O
SO_4^{2-}	<30 ppb

5.2.1 Air (1) and Air (3) tests

Figures 5.5 and 5.6 show the da/dN versus ΔK curves for tests AIR (1) and AIR (3). The two curves have been superimposed in Fig. 5.7 and it can be seen that decreasing the frequency of testing (in air) from 10 Hz to 1 Hz has had no effect on the crack growth rate of SA508 C13 steel. Clearly, both curves lie below the ASME XI (1980) crack growth rate curve for a subsurface flaw, tested in air.

As can be expected, both the air tests produced similar fracture surfaces. Plates 5.18 - 5.20 show the fracture mode to be ductile and only in certain regions have inclusions been observed. However, these inclusions have not interfered with the crack growth mechanism (i.e. no brittle - fast fracture regions about the inclusions). However, the crack growth would be affected by the presence of inclusions which would 'weaken' the matrix in the vicinity of the inclusion, since MnS is a non-coherent precipitate. The length of inclusion would lead one to assume that the inclusions are of Type II [51]. (Plate 5.21 shows an EDAX analysis of the inclusions.) Clearly they are MnS and indeed, all the inclusions found on the fracture surfaces (P.W.R. environment tests as well) were identified as MnS.

In general, the two air test fracture surfaces were found to be quite clean (i.e. few MnS inclusions) and the MnS inclusions were found to lie normal to the crack growth direction.

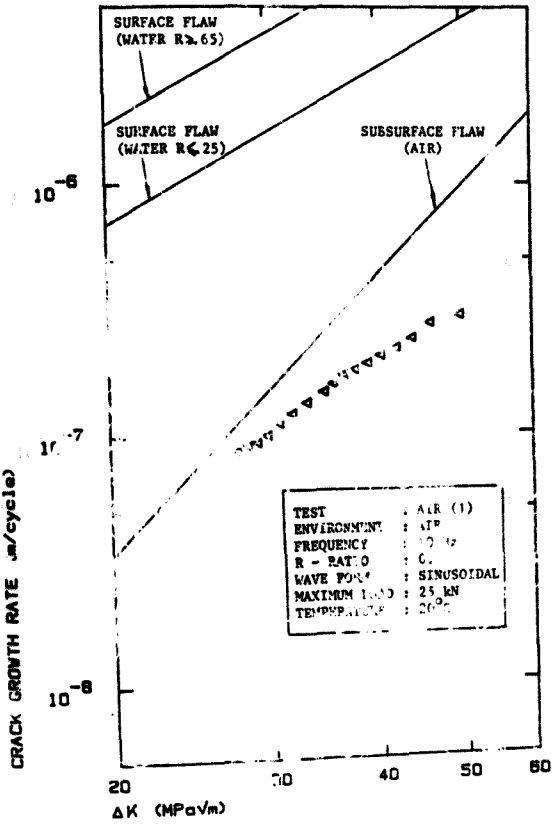

FIGURE 5.1: da/dN versus ΔK curve for test AIR (1)

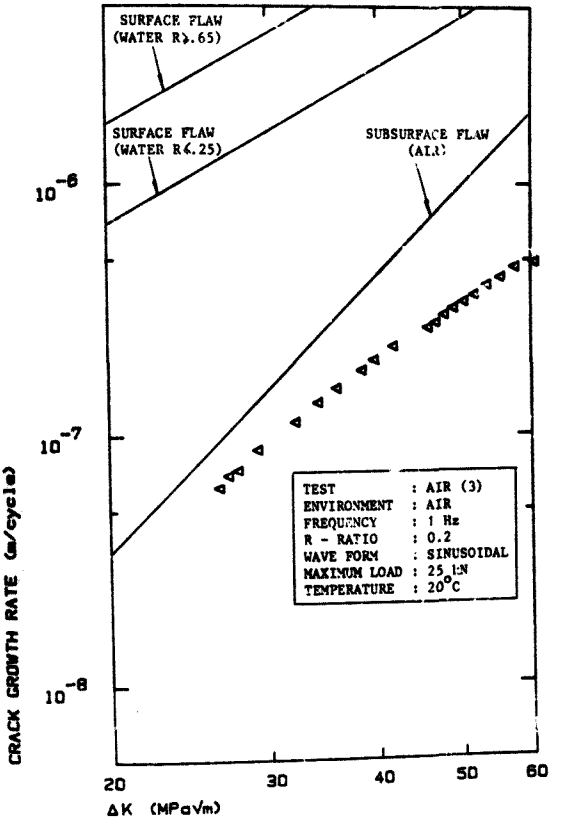

FIGURE 5.6: da/dN versus ΔK curve for test AIR (3)

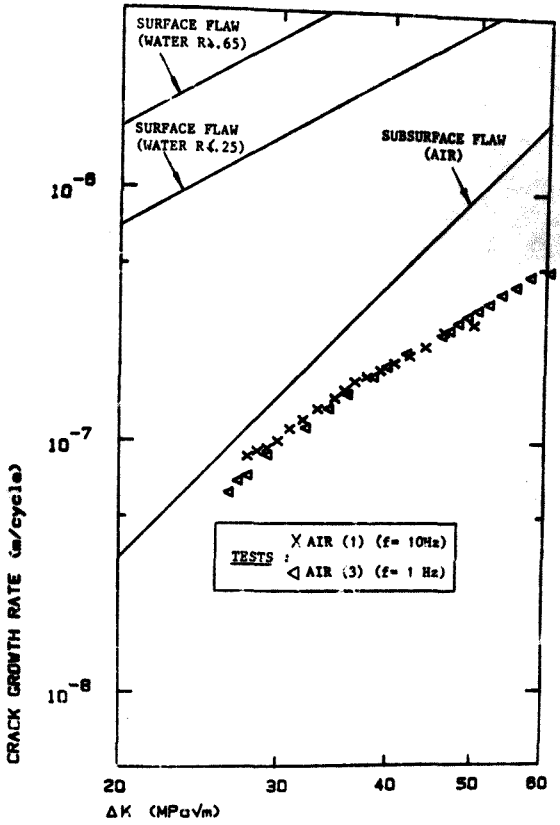

FIGURE 5.7: Combined da/dN versus ΔK curves for tests AIR (1) and AIR (3)

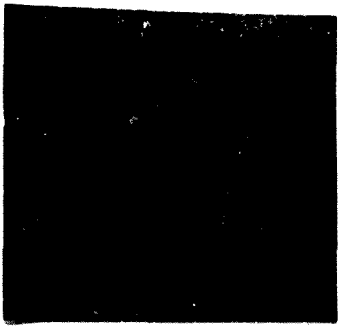

PLATE 5.18: General fracture surface showing MnS inclusion sites. (Mag. x 20). Crack growth is always from the bottom of the Plate to the top.

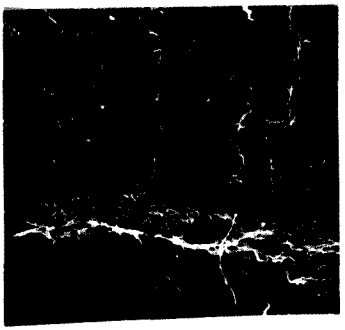

PLATE 5.19: 'Broken-up' MnS inclusion. Fracture mode similar before and after the MnS. (Mag. x 500)

PLATE 5.20: MnS stringer region only affecting crack growth locally. (Mag. x 100)

PLATE 5.21: MnS stringer EDAX analysis showing no traces of other elements.

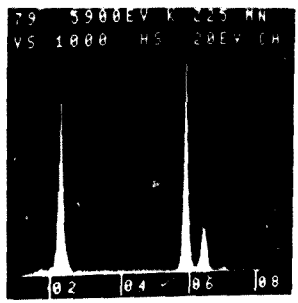

PLATE 5.20: MnS stringer region only affecting crack growth locally. (Mag. x 100)

PLATE 5.21: MnS stringer EDAX analysis showing no traces of other elements.

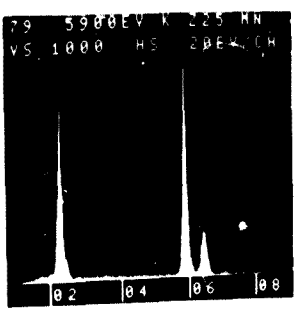

5.2.2 P.W.R.(1a) and P.W.R.(1b) tests

These two tests served as a basis for all the subsequent tests. The da/dN versus ΔK curves are given in Figs 5.8 and 5.9, and Fig. 5.10 shows the above two curves superimposed upon the air test data.

Clearly, both P.W.R. environment tests fall well below the ASME curve for an R-ratio <0.25 and only for low ΔK values do the curves lie above the air line data. It must be remembered that the ASME wet lines apply to testing at elevated temperatures (typically 288 °C) in P.W.R. environments. It is also important to note that P.W.R. water shows an effect (elevated da/dN versus ΔK plot with respect to air line data) for 10 Hz tests. As the frequency is decreased to 1 Hz, the fatigue crack growth rate increases for any given ΔK.

S.E.M. fractographs for test [illegible] shown in plates 5.22 - 5.26. Regions of fast crack [illegible] seen after the inclusion (plate 5.24) and in some cases [illegible] inclusions (plate 5.25). Plate 5.24 shows a typical inclusion site which has influenced crack growth up to 15 μm after the inclusion. The edge effect of the inclusion is clearly visible.

Plates 5.27 - 5.30 show the fractographic features found for specimen P.W.R. 1(b). Clearly the fracture mode is the same, i.e. ductile striation. Plate 5.27 shows a broken-up MnS not really affecting the crack growth rate (crack growth direction is always from the bottom of the photo to the top), since regions between the inclusion have failed by a ductile striation mechanism.

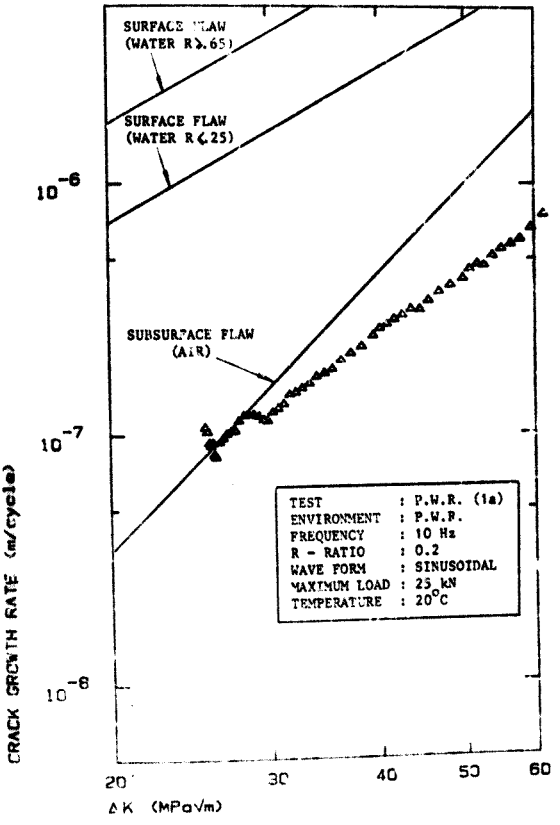

FIGURE 5.8: da/dN versus ΔK curve for test P.W.R. (1a)

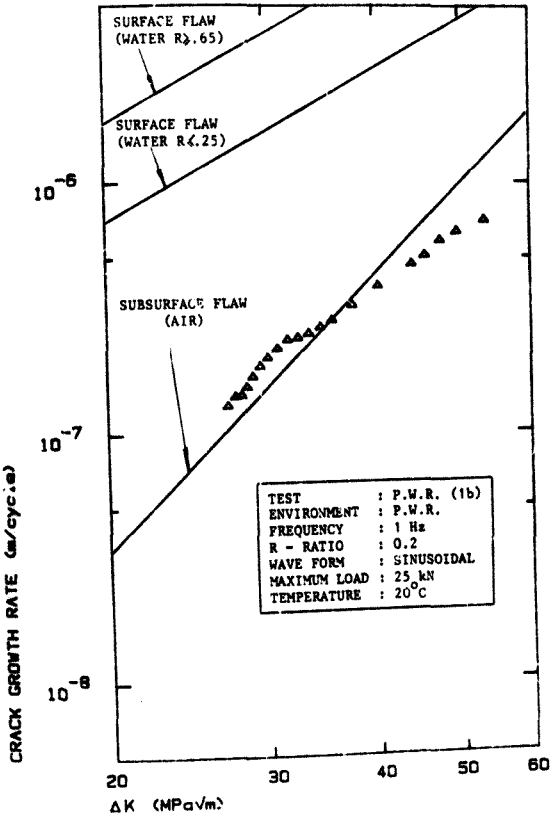

FIGURE 5.9: da/dN versus ΔK curve for test P.W.R. (1b)